sustainability

MDPI

Article

Studying the Impact of Urban Management Strategies and Spatiotemporal Dynamics of LULC on Land Surface Temperature and SUHI Formation in Jeddah, Saudi Arabia

Yehia Miky [1,2,*], Ahmed Al Shouny [1,3] and Ashraf Abdallah [2]

[1] Geomatics Department, Faculty of Architecture and Planning, King Abdulaziz University, Jeddah 21589, Saudi Arabia
[2] Civil Engineering Department, Faculty of Engineering, Aswan University, Aswan 81528, Egypt
[3] Survey Research Institute, National Water Research Center, Giza 13411, Egypt
* Correspondence: yhhassan@kau.edu.sa; Tel.: +966-541463903

Abstract: This study focuses on examining the historical trends of the surface urban heat island (SUHI) in relation to land use/cover (LULC) changes in Jeddah City from 2013 to 2022 using Landsat data. To achieve this, various parameters were analyzed, including LULC changes, normalized difference built-up index (NDBI), normalized difference vegetation index (NDVI), and LST. During this timeframe, Jeddah City underwent a comprehensive development initiative aimed at demolishing informal and illegal settlements and improving the overall quality of life, aligning with the Kingdom's 2030 vision. This provides an interesting opportunity to investigate the effect of these urban transformations on the variation, presence, and intensity of SUHIs. Based on the results, a significant positive correlation between the density of built-up and LST was found, while a negative relationship was noticed between NDVI and LST for all time points. Furthermore, a remarkable observation in 2022 was the complete absence of the SUHI phenomenon following the removal of old informal settlements from the city. The outcomes of this study highlight the impact of urban development and hold the potential to uncover environmental imbalances and contribute to the development of strategies to mitigate the negative effects of LULC changes, thereby restraining the rise in LST.

Keywords: LULC dynamics; SUHI; LST; NDVI; NDBI; Jeddah

check for updates

Citation: Miky, Y.; Al Shouny, A.; Abdallah, A. Studying the Impact of Urban Management Strategies and Spatiotemporal Dynamics of LULC on Land Surface Temperature and SUHI Formation in Jeddah, Saudi Arabia. *Sustainability* **2023**, *15*, 15316. https://doi.org/10.3390/su152115316

Academic Editor: Fernando António Leal Pacheco

Received: 20 September 2023
Revised: 17 October 2023
Accepted: 24 October 2023
Published: 26 October 2023

Copyright: © 2023 by the authors. Licensee MDPI, Basel, Switzerland. This article is an open access article distributed under the terms and conditions of the Creative Commons Attribution (CC BY) license (https://creativecommons.org/licenses/by/4.0/).

1. Introduction

Urbanization is considered as one of the most important processes that affects the environment on local, regional, and global levels [1]. The construction projects or increasing buildings involved in urbanization often with vegetation removal, lead to increased heat absorption in urban centers. Urbanization transforms natural landscapes into artificial surfaces, altering surface energy budgets, changing physical surface properties, and modifying the hydrological cycle [2]. As a result, significant landscape changes occur, and one of the outcomes of this process is the creation of the surface urban heat island (SUHI), which refers to areas with higher temperatures than their surrounding regions.

Temperature itself plays a vital role in climate as it influences various human activities, including agriculture, housing, and tourism. Due to its close association with other climate elements, temperature is considered the driving force behind them. The interdependence among these elements means that they significantly impact each other [3]. When temperature changes, it can trigger a chain reaction of impacts across various climate variables. The combination of rising temperatures or extreme heat events and air pollution in urban areas poses a severe threat to human health, as indicated by [4]. Furthermore, localized synergies between heat waves and urban heat island effects have significant implications on human thermal comfort and urban heat management [5]. As it is classified as a localized phenomenon, SUHI is sensitive to local variations in thermal, aerodynamic, moisture [6],

land use dynamics [7,8] and urban development and typology [9]. The challenges posed by urbanization and climate change are diverse and affect cities globally [10].

The SUHI effect is widely acknowledged as a prominent feature of the urban climate. One crucial parameter in the physical processes of the Earth is Land Surface Temperature (LST), as noted in [11]. However, obtaining thermal images with high spatial, radiometric and temporal resolution is currently challenging due to the limitations of thermal infrared sensors [12]. Nonetheless, it is possible to calculate LST using different sources of surface emissivity from thermal infrared sensors such as that on Landsat 5, 7, 8, and 9 [13,14], MODIS, ASTER, and ECOSTRESS.

Land use/land cover (LULC) changes in urban settings are a crucial aspect that physically impacts the Earth's surface. The distinctive physical characteristics of each LULC category regarding radiation and energy absorption contribute to this effect [15–17]. Thus, any alterations in LULC patterns will result in a shift in energy exchange between the atmosphere and the ground surface. This, in turn, will bring about modifications in aerodynamic balance, as observed in [15,18–20]. Satellite images are usually used for the registering and mapping of LULC changes [14,21,22]. The use of satellite-derived imagery datasets provides a medium to high-resolution scene and permits continuous monitoring of the Earth's surface and atmosphere. This has been extensively leveraged to obtain the data required to monitor recent alterations in LULC and its impact on SUHI. Numerous studies have explored the correlation between LST and LULC using remote sensing imagery and geographic information systems (GIS) at the local and global levels [23–29]. Recently, spatiotemporal analysis of SUHIs in relation to urban development of different cities was presented [30–34].

Jeddah city is located in an arid and semi-arid area, and it receives great governmental attention regarding pelleting and development. In 2021, hoping to achieve high-quality urbanizing trends, a comprehensive development process was initiated in the city of Jeddah, which included removing informal and illegal settlements and buildings without an identity or architectural character, with the aim of serving humanity and ensuring sustainable development. Infrastructure is being developed and services and projects are being created to improve the quality of life in accordance with the Kingdom's 2030 vision [35]. Exactly 34 neighborhoods in different areas were removed, with a total area of 37.703 Km^2 [36], and these areas have become open spaces. As a result, the land cover in Jeddah has been greatly affected. Consequently, LULC dynamics have dramatically altered in the last three years in this city. The main reasons behind choosing Jeddah city as a case for our study are: (1) the comprehensive urban development process for quality-of-life improvement through demolishing the informal and illegal settlements in Jeddah; (2) the investigation of localized synergies between LULC dynamics and LST and its implications on SUHIs formation. The question we aim to address in this study is: to what extent do the new urban strategies influence the LST in Jeddah? Therefore, the objectives of this study are as follows: first, to track the dynamics of LULC changes and their impact on LST within the city of Jeddah; second, to efficiently evaluate the phenomenon of SUHI; and third, to investigate the relationships between LULC changes and SUHI during the period from 2013 to 2023 using remote sensing and GIS techniques.

2. Materials and Methods

2.1. Study Area

Jeddah is the second largest city in Saudi Arabia. It is located on the west coast of Saudi Arabia at latitude 29.21° north and longitude 39.7° east, as shown in Figure 1. As of 2023, the estimated population of Jeddah city was around 14% of the total population of the Kingdom (about 4.86 million people) [37]. While the municipal area of Jeddah covers 5460 km^2, the total urban area in Jeddah is about 1765 km^2 [38]. Terrain elevations in Jeddah range from 0 m to 265 m above mean sea level. Saudi Arabia has a desert climate. It is characterized by extreme heat in the daytime and a sharp decrease in temperature at night, with inconsistent rainfall patterns. Also, there is a considerable temperature and humidity

variation across the country, as a result of the influence of a subtropical high-pressure system and varying elevation. Unlike other Saudi Arabian cities, Jeddah features an arid climate, it is very hot in summer and preserves its warm temperature in winter. Summer temperatures are extremely hot (more than 48 °C in the afternoon and about 35 °C in the evening). In winter, it ranges from 15 °C at dawn to 28 °C in the afternoon. Recently, a comprehensive development process was initiated in Jeddah city to achieve high-quality urbanizing trends to improve the quality of life. The LULC in Jeddah has been greatly affected by the removal of neighborhoods. This makes the investigation of the influence of these changes on LST very necessary.

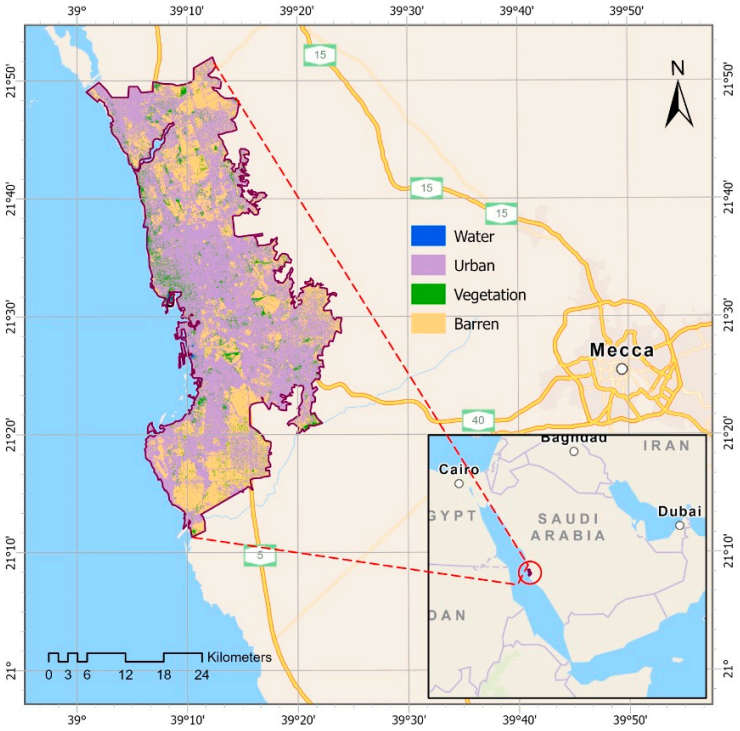


Figure 1. Location map of the study area, Jeddah city.

2.2. Urban Management Strategies

Urban management strategies, often conducted by governments, aim to enhance people's quality of life and address the challenges posed by rapid urbanization, population growth, and resource management in cities. These strategies involve the formulation of action plans, efficient implementation, monitoring, and evaluation procedures to achieve development goals [39,40]. Urban development strategies are constantly evolving to address emerging issues, such as climate change, within the global urban landscape.

Since the 1970s, urban development has been an integral aspect of Saudi Arabia's national development policy [41]. In 2015, the Council of Economic and Development Affairs introduced a new strategy with a goal to create highly efficient urban environments across the Kingdom, promoting balance and sustainability in urban development [42]. Furthermore, the Kingdom of Saudi Arabia embarked on a comprehensive national development strategy, Vision 2030, in 2016. This ambitious vision outlines significant goals for the nation and emphasizes the need for substantial reforms in the public sector, economy, and society at large. These reforms include enhancing the quality of urban development, improving city performance, and raising the quality of life for Saudi citizens and visitors to the country.

2.3. Data Source and Preprocessing

The Landsat 8 OLI/TIRS images provided by the United States Geological Survey (USGS) were used in this research to investigate the impact of LULC changes on LST between 2013 and 2022. The details of the Landsat datasets used in this study are shown in Table 1. A total of 36 images were selected, taken during the summer season when cloud cover is minimal in the region (three to four images per year, depending on availability). To ensure accurate image comparisons, all images were subjected to the necessary radiometric calibrations which are entirely depending on the sensor characteristics, atmospheric corrections and geometric registration to rectify the various surface reflectance variations. Landsat images were atmospherically corrected in ENVI software using the fast line-of-sight atmospheric analysis of spectral hypercubes algorithm (FLAASH). The pre-processed visible light bands were utilized to map LULC, normalized deference vegetation index (NDVI), and normalized difference built-up index (NDBI) while, the thermal infrared band 10 was used for LST estimation. Due to the larger uncertainty in the band 11 values, as mentioned in the Landsat 8 User's Handbook, only data from band 10 are suitable for LST retrieva1 [3,43]. The ground truth was picked out using Google Earth imagery. Additionally, the obtained results were compared with past temperature information downloaded free of charge from the King Abdulaziz airport meteorological station [44].

Table 1. Details of Landsat datasets of the Jeddah Region.

Year	Product Identifier	Sensing Time (hh:mm:ss)	Cloud Cover Land (%)	Background Temp. (°C)	Wind Speed km/h	Sun Azimuth	Sun Elevation
2013	LC08_170045_20130521	07:51:11.89	0.00	29	0	89.8569	69.1416
	LC08_170045_20130622	07:51:04.89	0.00	29	7	80.8680	68.1214
	LC08_170045_20130724	07:51:08.28	0.13	29	0	90.0961	66.7928
	LC08_170045_20130809	07:51:10.53	0.58	31	7	100.0579	66.0791
2014	LC08_170045_20140609	07:48:50.89	0.01	28	6	82.2194	68.2251
	LC08_170045_20140625	07:48:52.82	0.85	29	7	80.9886	67.4774
	LC08_170045_20140711	07:49:01.67	0.00	29	7	84.2406	66.7866
	LC08_170045_20140812	07:49:13.29	0.09	31	11	101.6443	65.4652
2015	LC08_170045_20150527	07:48:14.34	0.00	30	0	86.8041	68.4841
	LC08_170045_20150628	07:48:31.85	0.00	27	7	81.2406	67.2550
	LC08_170045_20150916	07:49:06.59	0.01	30	7	127.9526	60.1340
2016	LC08_170045_20160513	07:48:42.10	0.00	28	9	94.2899	68.3384
	LC08_170045_20160716	07:49:07.68	0.80	30	17	86.3003	66.6029
	LC08_170045_20160902	07:49:21.67	0.92	31	11	118.1130	63.4131
2017	LC08_170045_20170703	07:48:57.27	0.00	31	15	82.1439	67.1009
	LC08_170045_20170804	07:49:09.30	0.65	31	7	96.3634	65.8763
	LC08_170045_20170820	07:49:14.42	3.16	33	9	107.7871	64.8663
2018	LC08_170045_20180519	07:48:08.01	0.00	28	4	90.8341	68.3970
	LC08_170045_20180604	07:47:56.83	0.15	28	6	83.5556	68.2336
	LC08_170045_20180722	07:48:23.00	0.00	31	11	88.7358	66.2386
	LC08_170045_20180807	07:48:31.73	0.00	31	11	98.0856	65.6072
2019	LC08_170045_20190506	07:48:38.42	0.00	29	7	99.4870	67.7398
	LC08_170045_20190607	07:48:56.62	0.00	31	6	82.7635	68.3271
	LC08_170045_20190826	07:49:21.02	3.47	30	7	112.0857	64.3652
2020	LC08_170045_20200524	07:48:37.08	0.01	29	0	87.8919	68.5838
	LC08_170045_20200625	07:48:54.29	0.00	28	11	81.0232	67.4365
	LC08_170045_20200711	07:49:01.11	0.00	30	11	84.4186	66.7612
	LC08_170045_20200828	07:49:17.71	0.00	30	6	114.2160	64.0352
2021	LC08_170045_20210511	07:48:42.55	0.00	28	0	95.7292	68.2017
	LC08_170045_20210527	07:48:52.47	0.13	30	9	86.5779	68.5985
	LC08_170045_20210628	07:49:03.49	0.00	30	15	81.3038	67.3361
	LC08_170045_20210831	07:49:23.54	3.61	30	4	116.3964	63.7145
2022	LC08_170045_20220514	07:49:05.60	0.04	32	6	93.9723	68.4412
	LC08_170045_20220615	07:49:20.60	0.01	29	11	81.1881	68.0301
	LC08_170045_20220717	07:49:24.60	2.00	30	7	86.5416	66.6412
	LC08_170045_20220818	07:49:42.12	0.57	31	6	106.1829	65.1197

2.4. Cloud-Computing Platform: Google Earth Engine (GEE)

Nowadays, with the availability of advanced robust techniques and the accessibility to cloud-computing platforms and algorithms, large-scale analysis and mapping can now be conducted at a low cost [45]. Google Earth Engine (GEE), as one of these platforms, offers a wealth of remotely accessed datasets, fully automated parallel processing, and powerful computational capabilities. It enables users to quickly filter and select their desired datasets by defining specific spatial and temporal parameters. Notably, users are not required to download any datasets for processing as all tasks can be performed within the GEE interface [46]. GEE provides a convenient environment for interactive data and algorithm development. It allows users to upload and manage their data and collections via a java script code, with all processing handled by Google's cloud resources. Consequently, this large data repository can now be mined more effectively than ever before by researchers and scientists for tasks such as mapping patterns, change detection, and quantifying resources on Earth's surface [47]. The platform includes several built-in algorithms for planetary-scale data analysis. It has immense potential for big data processing across a variety of disciplines [45]. In addition to ENVI5.3 and ArcGIS Pro software, https://www.arcgis.com/index.html, this study employs the GEE platform for supervised classification of Landsat images and for SUHI delineation.

2.5. LULC Classification and Change Detection

To retrieve the LULC variations, ten Landsat 8/THIR images were utilized for different time-points: one image for each year from 2013 to 2022, taken in the same month. The Random Forest algorithm was used to generate the LULC maps through a supervised classification process. The classification was performed on the GEE platform [48]. The output maps were classified into four broad categories of water, urban, vegetation, and barren lands. Water areas comprise sea, ponds, lakes, and wetland areas. The urban class represents all commercial, residential, industrial, and other facilities related to urban infrastructural. The vegetation class denotes trees, agricultural lands, and all other grass-cover areas, while the city's non-inhabited areas were shown as barren land.

To assess the accuracy of the LULC classification, a stratified random sampling method was used to select sample points of the study area for each year. The samples were compared with independent reference data, separate from the points used for training during image classification. The selected number of random validation points in each category corresponds to the relative size of the corresponding category, with the total number of 851 points spatially distributed over the study area. Reference data were approved based on Google Earth imagery. The results were statistically analyzed using the confusion matrix approach. The overall accuracy indicator was used to represent the accuracy achieved. However, the Kappa coefficient, as it is not an index for accuracy [49], is calculated for evaluating the agreement in class labelling.

Thematic change detection was performed using ENVI5.3 software to compare the classification maps of each consecutive pair of years, from 2013 to 2022. The area of changes between different classes were calculated. The areas of changes from urban to barren soils and from barren soils to urban in the LULC maps were calculated and then linked with changes in land surface temperature to estimate the degree of correlation between changes in land surface temperature associated with changes in LULC.

2.6. Land Surface Temperature (LST) Retrieval

In this study, a single channel approach was utilized to retrieve the LST. The information of thermal infrared band 10 of the Landsat 8 thermal sensor (THIR) was employed to retrieve and map the study area's LST. To eliminate atmospheric effect from thermal infrared images using ENVI 5.3 software, it is essential to take into account the following assumptions: (1) the atmospheric conditions are consistent across the entire data scene; (2) uniform emissivity is assumed for all features; (3) there is no presence of reflected downwelling radiance; (4) a near-blackbody surface exists within the scene. The procedure

for extracting temperature values from the digital numbers (DNs) is outlined in the Landsat 8 User's Handbook [43] and can be simplified into several steps. Initially, the DNs are transformed into radiance using the following formula:

$$L_\lambda = M_L \times Q_{cal} + A_L \quad (1)$$

where L_λ represents the top of atmosphere (TOA) spectral radiance in (W/(m^2 × sr × µm)); M_L is the multiplicative scaling factor, obtained from the metadata for radiance; A_L is the additive scaling factor obtained from the metadata for radiance; Q_{cal} is the image pixel value.

Then, the effective at-satellite temperature of the viewed Earth-atmosphere system under the abovementioned assumptions could be obtained from the above spectral radiance by following formula [23,50,51]:

$$T_B = \frac{K_2}{\ln(\frac{K_1}{L_\lambda} + 1)} \quad (2)$$

where T_B represents the TOA brightness temperature, in Kelvin; L_λ is the spectral radiance in (Watts/(m^2 × sr × µm)); K_1 and K_2 are the retrieved metadata's thermal conversion constants obtained from the metadata.

The next step is to derive the LST from brightness temperature, T_B. To do so, we need first to calculate the emissivity values (ε) using the following equation [25,52].

$$\varepsilon = m\, P_v + n \quad (3)$$

where ε is the land surface emissivity, n = 0.004, m = 0.986, and P_v is the proportion of vegetation that can be calculated as Equation (4) [26,51].

$$P_v = \left(\frac{NDVI - NDVI_{min}}{NDVI_{max} + NDVI_{min}}\right)^2 \quad (4)$$

where NDVI is one of the major indicators to quantify vegetation cover and it can be calculated from the red and near-infrared bands using the following equation.

$$NDVI = \frac{\rho_{NIR} - \rho_{RED}}{\rho_{NIR} + \rho_{RED}} \quad (5)$$

where ρ_{RED} refers to surface reflectance of the red band, Band (4) in Landsat OLI (0.64–0.67 µm), and ρ_{NIR} refers to surface reflectance of the near infrared band, Band (5) in Landsat OLI (0.85–0.88 µm). Finally, LST in Celsius can be estimated by Equation (6).

$$LST = \left(\frac{T_B}{1 + \lambda\left(\frac{T_B}{\rho}\right)\ln(\varepsilon)}\right) - 273.15 \quad (6)$$

where λ is the wavelength of emitted radiance of Landsat 8, band 10 = 10.8 µm, $\rho = h\left(\frac{c}{\sigma}\right)$, h is Planck's constant (6.626 × 10^{-34} Js), c is the velocity of light (2.998 × 10^8 m/s), and σ is Boltzmann constant (1.38 × 10^{-23} J/K).

When the LST result for each image is calculated, it is possible to estimate the average summer LST of the study area for each year [27].

To assess the accuracy of the LST estimation, we compared the historical temperature data collected from the meteorological station situated at King Abdulaziz Airport, which is accessible online, with the LST results obtained for the same location during the corresponding scene times. The King Abdulaziz Airport station offers detailed hourly temperature information, although, for archival purposes, temperature data is recorded and reported four times daily [44]. Therefore, the temperature range recorded between

6:00 a.m. and 12:00 p.m. was utilized for comparison with the daytime satellite images captured in the early morning.

2.7. Satellite Derived Indices (NDVI) and (NDBI)

The normalized difference vegetation index (NDVI) is a key indicator for studying vegetation and urbanization in environmental studies. It is a standardized measure that ranges from −1 to +1, where higher positive values indicate vegetation presence, lower positive values indicate built-up areas or bare soils, and negative or near-negative values indicate water bodies or adjacent areas [53]. In this study, NDVI was used to calculate the proportion of vegetation in Equation (4). Also, it was employed to establish its correlation with the derived LST. To calculate NDVI, Equation (5) was used, which involves the red band (RED) and near-infrared band (NIR) [33,54].

The normalized difference built-up index (NDBI) is a significant indicator for monitoring the urban and environmental conditions [33,53]. It is an effective technique for analyzing and mapping land-use patterns by providing valuable information on the spatial distribution of built-up areas and impervious surfaces. NDBI quantifies the density of built-up areas within individual pixels, with values ranging from −1 to +1. Negative values typically indicate the presence of vegetation, while positive values represent built-up urban areas [33,53]. It was estimated to investigate the degree of correlation with the derived LST. To calculate NDBI, Equation (7) was used, which involves the NIR band and the shortwave-infrared (SWIR).

$$\text{NDBI} = \frac{\rho_{SWIR} - \rho_{NIR}}{\rho_{SWIR} + \rho_{NIR}} \tag{7}$$

where ρ_{NIR} refers to surface reflectance of the near infrared band, Band (5) in Landsat OLI (0.85–0.88 µm), and ρ_{SWIR} refers to surface reflectance of short-wave infrared band, Band (6) in Landsat OLI (1.57–1.65 µm).

2.8. Retrieval of Surface Urban Heat Islands

To obtain the LST ranges as an input parameter to detect the SUHI, the retrieved LSTs were normalized according to Equation (8). According to the rules shown in Table 2, the results were divided into seven intervals and the corresponding LSTs were identified for each interval.

$$\text{LST}_N = \left(\frac{\text{LST} - LST_{min}}{LST_{max} - LST_{min}} \right) \tag{8}$$

Table 2. Rules for dividing the intervals and ranges of land surface temperature (LST) [31].

Interval of LST	Range of LST (°C)
Low temperature	$LST_N < T_{avg} - 2.5\sigma$
Sub-low temperature	$T_{avg} - 2.5\sigma \leq LST_N < T_{avg} - 1.5\sigma$
Sub-medium temperature	$T_{avg} - 1.5\sigma \leq LST_N < T_{avg} - 0.5\sigma$
Medium temperature	$T_{avg} - 0.5\sigma \leq LST_N < T_{avg} + 0.5\sigma$
Sub-high temperature	$T_{avg} + 0.5\sigma \leq LST_N < T_{avg} + 1.5\sigma$
High temperature	$T_{avg} + 1.5\sigma \leq LST_N < T_{avg} + 2.5\sigma$
Extreme-high temperature	$T_{avg} + 2.5\sigma \leq LST_N$

LST is the land surface temperature, T_{avg} = is the average LST_N, and σ is the standard deviation.

Thus, the spatial distribution of LST classes was established, and the exact area for each class was determined according to intervals shown in Table 2.

In general, SUHI can be defined as the difference in surface temperature between the urban center and the countryside [55]. The approaches employed to quantify SUHIs can be classified into two main categories: the first category is based on the calculation of SUHI intensity defined as LST differences between urban and less developed areas, and the second consists of methods using retrieved LST as a proxy [56]. In the first approach, the temperature of the region beyond the urban boundary and that has the same area as the urban area, is considered as the background temperature. The average LST within this region is used as the background temperature. This may vary in arid and semi-arid regions, where there are no boundaries between urban and rural areas. For example, in the study area of this research, Jeddah city is bordered by the Red Sea to the west and the desert to the east, with vast open spaces interspersed with urban areas and a lack of vegetation and trees. Consequently, determining the centers of SUHI, its footprint, and its intensity with the first method is not an easy task. Therefore, since our study focuses on understanding the links between LULC Changes and LST and considering that the calculated temperature is the average temperature of the summer, we will use the second approach and consider the points belonging to the class of extreme-high temperature as the center of SUHI with a spatial extent of a 5 km radius circle [57].

To depict the variation of the intensities of UHIs in the study area and to assess the contribution of LULC, the urban heat island ratio index (URI) will be estimated for all time-points selected according to Equation (9) [32,51].

$$\mathrm{URI} = \frac{1}{100m} \sum_{i=1}^{n} w_i p_i \tag{9}$$

where i is the interval of temperature higher than medium, n is the number of LST intervals higher than the medium interval, m is the number of normalized LST intervals, w_i is the weighted value using higher than medium intervals, and p is the per cent of i.

2.9. Correlation Analysis

Generally, the objective of the correlation analysis typically aims to investigate and quantify the relationships and associations between variables within a specific geographical area or dataset. In this study the variables are LST, NDVI and NDBI, their associations will be investigated within the study area during the period from 2013 to 2022. A quantitative analysis was conducted to assess the individual variations in LST across different LULC categories. These LULC categories were determined through visual interpretation of classified maps, including water, urban areas, vegetation, and barren lands. The process involved converting the pixel values of LST into point data. Parametric values associated with these points were extracted from LST maps. These values were then utilized for comparison by overlaying them with the LST values corresponding to the chosen LULC categories. linear regression analysis using scatter plots was performed to examine the relationship between LST, NDVI and NDBI indices. The flow chart illustrated in Figure 2 summarizes the methodology used in this study.

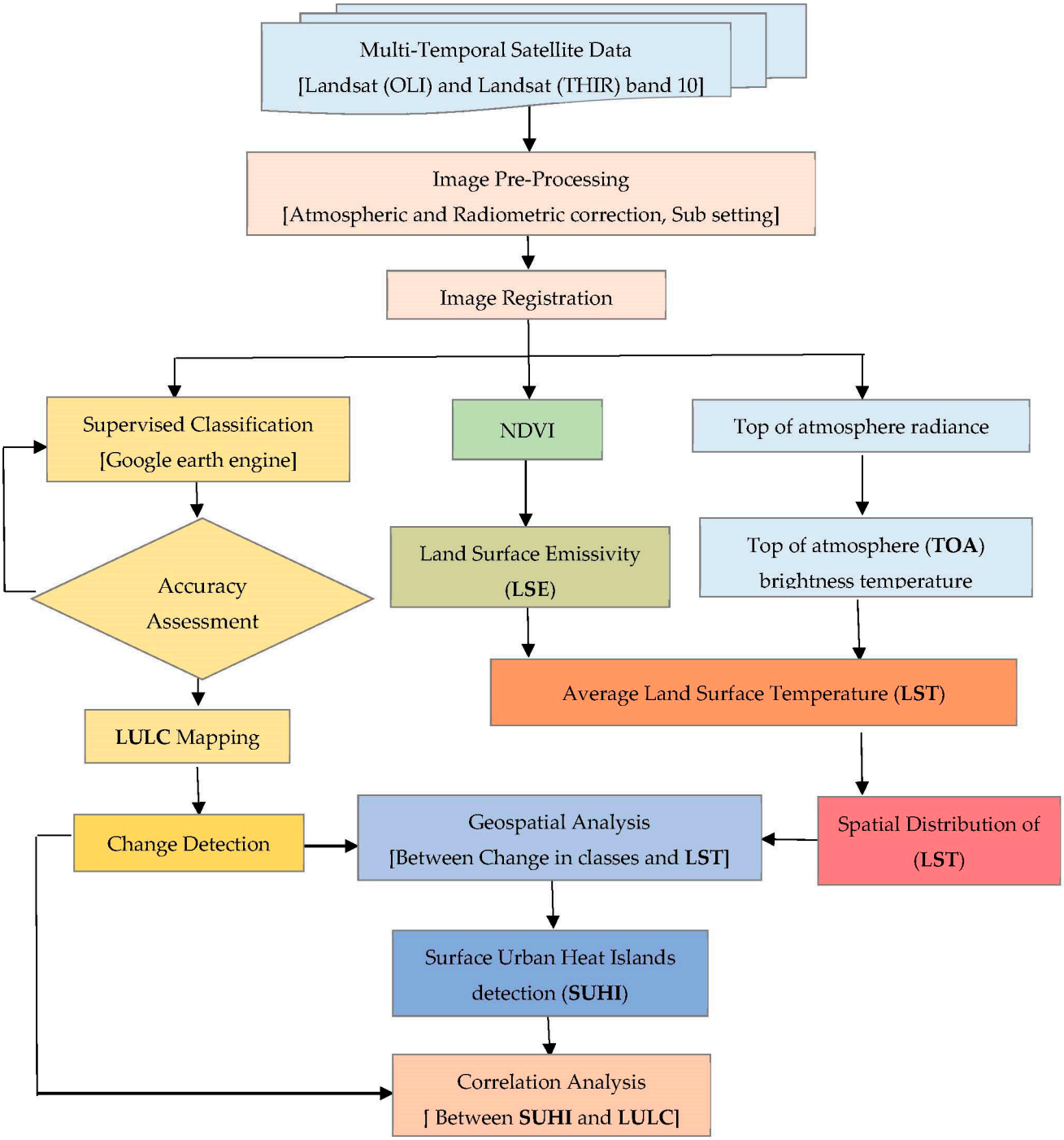


Figure 2. A typical workflow of the proposed methodology.

3. Results

3.1. Landsat Image Classification and Accuracy Assessment

The study area covers approximately 1231.72 km^2. The LULC were classified into four types as shown in Section 2.5 which are: water, urban, vegetation, and barren lands. The classified land cover maps of Jeddah for the different time points during the period from 2013 to 2022 are presented in Figure 3 and Appendix A and quantified in Table 3. Regarding water class, there is no significant change during the study period. The area of water within the study area ranged from 8.19 km^2 in 2014 to 10.72 km^2 in 2019. In the context of urban development in arid regions, an interesting pattern emerges. Specifically, within the study area, which is characterized as an arid region, the vegetation class covers

a small area in Jeddah city, expanding from 53.47 km^2 in 2013, to 65.70 km^2 in 2022. The other two classes, urban and barren lands, have shrunk and expanded in a compensatory manner due to the comprehensive development process in Jeddah city in recent years. This means that in some places, urban areas were converted to barren land, while in other places, barren areas were converted to urban. In summary, in 2013, the urban area was observed to be 764.15 km^2, and by 2022, there was a gain in urban occupation, reaching an area of 814.86 km^2. In parallel, barren land was reduced from 404.47 km^2 to 342.44 km^2.

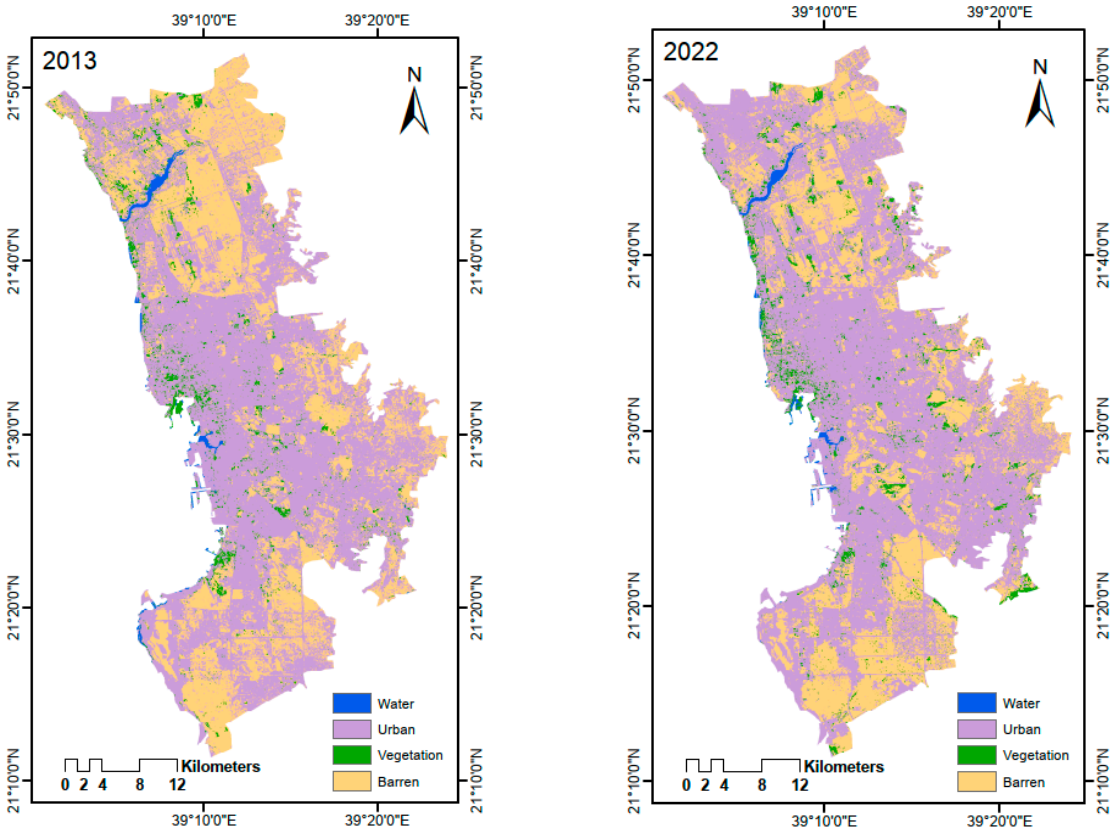


Figure 3. Spatial LULC in Jeddah city, map for 2013 and 2022.

Table 3. LULC distribution over the study area from 2013 to 2022.

Year	Water		Urban		Vegetation		Barren	
	Area (km^2)	Area (%)	Area (km^2)	Area (%)	Area (km^2)	Area (%)	Area (km^2)	Area (%)
2022	8.72	0.71	814.86	66.16	65.70	5.33	342.44	27.80
2021	8.34	0.68	766.08	62.20	47.65	3.87	409.66	33.26
2020	8.29	0.67	772.88	62.75	43.76	3.55	406.79	33.03
2019	10.72	0.87	674.17	54.73	48.38	3.93	498.45	40.47
2018	10.14	0.82	738.47	59.95	42.86	3.48	440.25	35.74
2017	10.11	0.82	746.08	60.57	38.57	3.13	436.96	35.48
2016	8.98	0.73	612.57	49.73	64.36	5.22	545.81	44.31
2015	8.83	0.72	717.54	58.25	47.86	3.89	457.50	37.14
2014	8.19	0.67	689.99	56.02	67.83	5.51	465.71	37.81
2013	9.64	0.78	764.15	62.04	53.47	4.34	404.47	32.84

The study area classifications were performed on the GEE platform using a supervised classification process with a Random Forest algorithm. The accuracy of LUCC was evaluated using a confusion matrix that shows correctly and incorrectly classified pixels. The accuracy assessment was calculated for each year, with approximately 100 randomly selected sampling points for each class compared with reference data selected based on Google Earth imagery each year. Table 4 summarizes the overall accuracy achieved as an index and the Kappa coefficient as an indicator of agreement in class labeling for all classifications. The overall accuracy for all classifications was not less than 95%, while the Kappa coefficient ranged between 0.84 and 0.934.

Table 4. Accuracy assessment for LULC classification of the study area from 2013 to 2022.

Classification	Overall Accuracy	Kappa
LULC-2022	0.972	0.914
LULC-2021	0.976	0.934
LULC-2020	0.979	0.933
LULC-2019	0.959	0.877
LULC-2018	0.966	0.892
LULC-2017	0.954	0.864
LULC-2016	0.961	0.882
LULC-2015	0.962	0.877
LULC-2014	0.951	0.840
LULC-2013	0.973	0.917

3.2. Change Detection Analysis

Change detection is a process of identifying, analyzing, and monitoring changes in LULC over time. The present study uses classified images to analyze annual LULC changes in Jeddah city between 2013 and 2022. The reason for choosing a time step of one year is the need to monitor small changes that may occur in the study area. These changes will be linked with LST to estimate the correlation between changes in LULC and LST. The LULC dynamics and temporal changes are quantified in Table 5 and presented in Figure 4. The study revealed notable heterogeneous spatiotemporal LULC changes during the period of study, showing both negative and positive changes in the various LULC classes. As the Red Sea was excluded from the study area and the amount of water inside the study area is small, the changes in the water over the ten years are negligible. Due to the fact that the study area is located in an arid region, the presence of vegetation is very low. Thus, the changes are also not significant and range between −1.47% and 2.09%. As shown in Figure 4, there is an inverse relationship between the urban area and the barren area. Any decline or shrinkage in the urban area is associated with an increase in the barren area. For example, between 2013–2014, the urban area of the city decreased by 48.78 km^2 while the barren area increased by 67.22 km^2. Similarly, between the periods 2015–2016, 2018–2019, and 2020–2021, the urban area decreased, and the barren area increased. The main reason behind the reduction in the urban area was the demolition of old, informal and illegal buildings. Conversely, between the periods 2014–2015, 2016–2017, 2017–2018, 2019–2020, and 2021–2022, the urban area expanded while the barren area shrunk. Observed change detection has diverse practical implications. In urban planning, it aids in identifying areas undergoing rapid urbanization or shifts in land use, crucial for infrastructure development and service provision. Additionally, it informs the adaptation of development regulations, facilitating controlled and sustainable expansion. In resource management, it plays a vital role in monitoring changes in water bodies, particularly significant in arid regions like Jeddah.

Table 5. LULC change dynamics of the study area from 2013 to 2022.

Period	Water		Urban		Vegetation		Barren	
	Area (km^2)	Area (%)	Area (km^2)	Area (%)	Area (km^2)	Area (%)	Area (km^2)	Area (%)
2013–2014	−0.38	−0.03	−48.78	−3.96	−18.05	−1.47	67.22	5.46
2014–2015	−0.05	0.00	6.8	0.55	−3.89	−0.32	−2.87	−0.23
2015–2016	2.43	0.20	−98.71	−8.01	4.62	0.38	91.66	7.44
2016–2017	−0.58	−0.05	64.3	5.22	−5.52	−0.45	−58.2	−4.73
2017–2018	−0.03	0.00	7.61	0.62	−4.29	−0.35	−3.29	−0.27
2018–2019	−1.13	−0.09	−133.51	−10.84	25.79	2.09	108.85	8.84
2019–2020	−0.15	−0.01	104.97	8.52	−16.5	−1.34	−88.31	−7.17
2020–2021	−0.64	−0.05	−27.55	−2.24	19.97	1.62	8.21	0.67
2021–2022	1.45	0.12	74.16	6.02	−14.36	−1.17	−61.24	−4.97

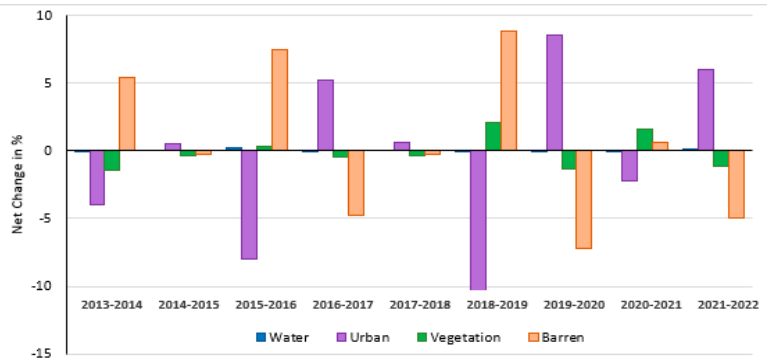


Figure 4. Net changes in LULC types in the study area during the study periods.

3.3. LST Distribution

Understanding LST distribution is very important in various fields such as urban planning, environmental science, climate studies, and agriculture. LST data helps identify areas with extreme temperatures, which is essential for urban planners to mitigate the SUHI effect. Furthermore, it gives valuable insights into SUHIs, LULC changes, and their relationship. Understanding the relationship between LST and LULC changes enables better monitoring and adaptation. For instance, urban planners can use LST data to assess the impact of urbanization on local temperature patterns and adapt accordingly.

The spatial distributions of LST in Jedda city from 2013 to 2022 were extracted as described in Section 2.5. The descriptive statistics of LST for different LULC classes in all years are presented in Table 6. This table describes the mean LST distribution over each distinct LULC class to study the dynamic effects of LULC on LST. The results indicate the range of LST values for the period from 2013 to 2022 as follows: 27.67–49.58 °C, 28.60–49.42 °C, 29.34–50.47 °C, 27.56–45.31 °C, 29.65–48.81 °C, 28.73–52.19 °C, 29.06–49.37 °C, 28.93–49.81 °C, 29.33–47.52 °C, and 28.77–47.05 °C. Additionally, the results reveal a significant increase in the mean LST of the urban class from 41.89 °C in 2013 to 44.36 °C in 2015, followed by a decrease from 43.09 °C in 2017 to 41.83 °C in 2022. As for the barren land class, there was an increase in the mean LST from 42.71 °C in 2013 to 45.75 °C in 2015. Similar to the urban class, the mean LST of the barren land class decreased from 44.41 °C in 2017 to 43.02 °C in 2022. Sometimes, relying solely on median and mean values may not provide a comprehensive understanding of a dataset. Questions may arise regarding the clustering of data and the presence of peaks within the distribution. In order to gain deeper insights into the distribution of LST across different LULC classes and highlight the peaks in the data, violin plots were employed. Figure 5 illustrates the violin plots of LST for various LULC classes over the period from 2013 to 2022. As shown in Table 7, an agreement was noticed when comparing the LST values estimated over King Abdulaziz airport during the scene time in the summer period with the past temperature information downloaded from the meteorological station at the airport. The average LSTs were normalized and divided

into seven temperature intervals as shown in Table 2. The results are illustrated in Figure 6 and Appendix B.

Table 6. Descriptive statistics of LST for different LULC classes in the studied years.

Y.	Land Cover	Min.	Mean	Max.	S.D	Median	Skewness	Kurtosis	NMAD
2013	Water	27.67	32.79	45.83	2.85	31.93	1.60	5.61	2.22
	Urban	28.18	41.89	49.58	1.89	42.07	−0.93	5.62	1.50
	Vegetation	29.21	41.30	47.11	2.27	41.54	−0.87	4.44	1.78
	Barren Land	30.83	42.71	47.27	1.48	42.92	−0.61	3.43	1.19
2014	Water	28.60	33.58	45.50	3.24	32.92	1.44	5.49	1.96
	Urban	29.31	42.92	49.42	1.93	43.15	−1.36	8.04	1.46
	Vegetation	30.23	42.98	49.24	2.23	43.35	−0.84	4.11	1.76
	Barren Land	30.19	44.01	48.39	1.56	44.08	−0.61	3.88	1.19
2015	Water	29.34	34.47	46.64	3.50	33.70	1.12	4.05	2.26
	Urban	30.06	44.36	50.37	1.91	44.63	−1.21	7.71	1.47
	Vegetation	31.84	43.74	50.20	2.35	43.98	−0.62	4.00	1.86
	Barren Land	31.40	45.75	50.47	1.42	45.84	−0.53	4.98	1.05
2016	Water	27.56	33.76	42.85	3.62	32.45	0.71	2.25	2.18
	Urban	28.62	39.61	45.31	1.50	39.77	−0.95	6.01	1.16
	Vegetation	28.84	39.64	45.29	1.83	39.92	−1.38	6.64	1.38
	Barren Land	30.67	40.64	45.21	1.06	40.77	−0.56	4.33	0.83
2017	Water	29.65	33.98	45.39	2.98	33.27	1.46	5.12	1.77
	Urban	30.05	43.09	48.81	1.79	43.27	−1.00	6.32	1.41
	Vegetation	30.11	42.81	48.34	2.36	43.32	−1.57	6.75	1.79
	Barren Land	33.06	44.41	47.98	1.26	44.47	−0.57	4.03	0.98
2018	Water	28.73	32.99	46.35	3.19	31.97	1.63	5.36	2.05
	Urban	29.56	42.95	52.19	1.88	42.62	−0.67	4.36	1.50
	Vegetation	30.26	42.49	52.06	2.65	42.83	−0.91	4.23	2.09
	Barren Land	31.07	43.61	51.83	1.51	43.66	−0.49	3.62	1.18
2019	Water	29.06	37.34	47.07	5.03	37.21	0.02	1.52	4.00
	Urban	29.26	42.81	48.73	2.03	43.07	−0.91	5.17	1.62
	Vegetation	29.16	43.00	48.75	2.45	43.51	−1.28	5.61	1.91
	Barren Land	32.06	44.32	49.37	1.57	44.50	−0.79	4.14	1.22
2020	Water	28.93	38.23	49.73	5.54	38.82	−0.08	1.42	4.61
	Urban	29.59	43.08	49.50	1.81	43.19	−0.81	5.60	1.42
	Vegetation	29.57	43.41	49.29	2.36	43.84	−1.54	7.03	1.78
	Barren Land	32.85	44.13	49.81	1.49	44.17	−0.47	3.78	1.15
2021	Water	29.33	34.90	45.94	4.04	33.56	1.01	2.91	2.18
	Urban	29.69	42.41	47.39	1.77	42.63	−1.08	6.42	1.40
	Vegetation	30.27	42.12	47.31	2.36	42.52	−1.05	4.69	1.84
	Barren Land	33.15	43.72	47.52	1.37	43.86	−0.61	3.87	1.07
2022	Water	28.77	35.57	45.45	4.19	34.68	0.87	2.87	2.73
	Urban	29.10	41.83	46.63	1.57	42.05	−1.14	7.39	1.25
	Vegetation	31.04	41.94	47.05	1.96	42.25	−0.88	4.158	1.58
	Barren Land	33.15	43.02	46.68	1.21	43.19	−0.89	4.33	0.95

Table 7. Temperature comparison over King Abdulaziz airport during scene times.

Temperature (°C)	24 July 2013	10 July 2014	28 June 2015	17 July 2016	03 July 2017	22 July 2018	07 June 2019	11 July 2020	28 June 2021	17 July 2022
Obtained from airport station	28–32	28–33	26–31	27–33	27–32	26–32	26–32	27–31	27–31	27–31
Calculated by the proposed method	28.63	29.11	30.56	29.08	31.33	30.22	29.11	30.26	30.32	29.81

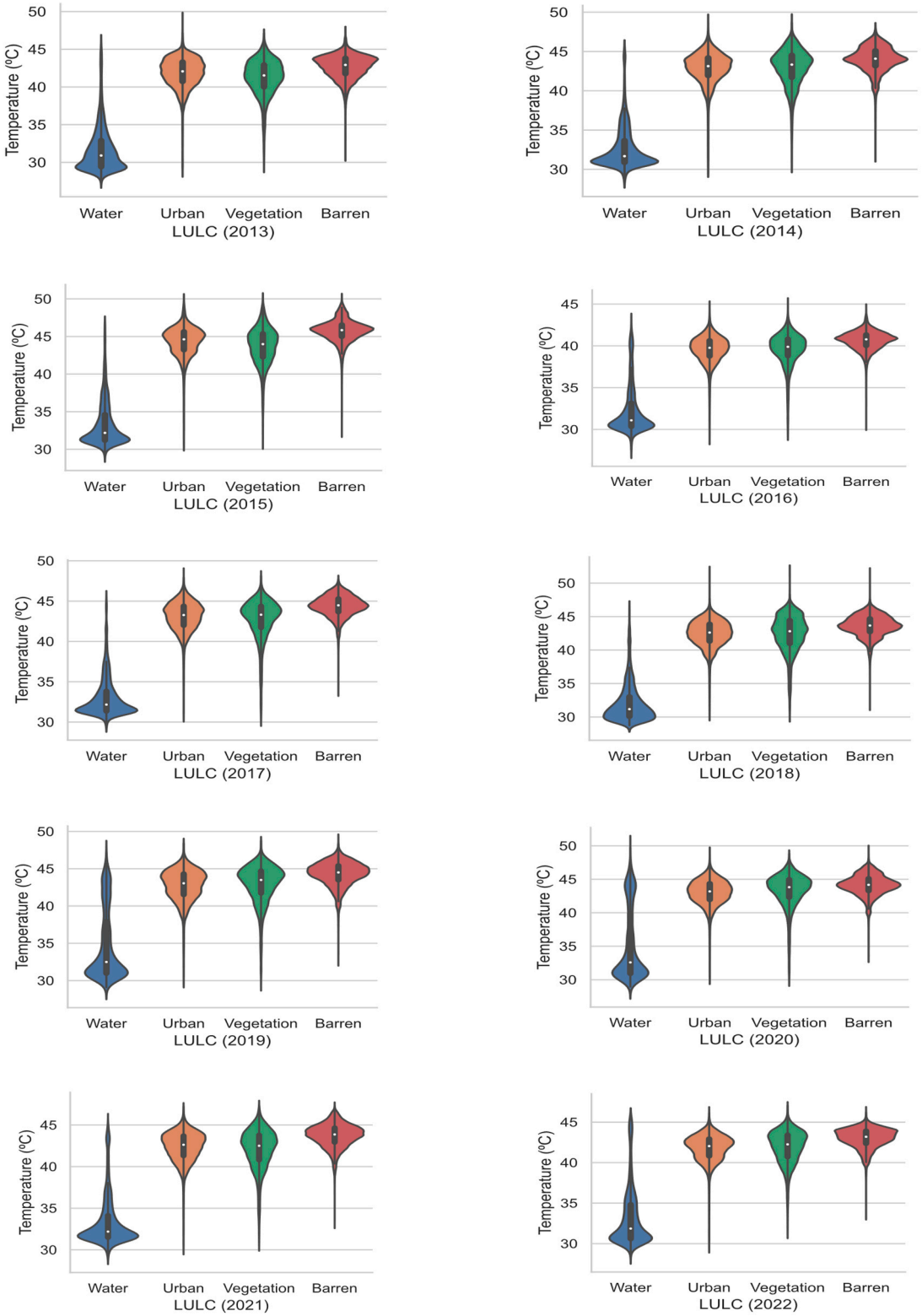


Figure 5. Violin plots of LST for different LULC during the period from 2013 to 2022.

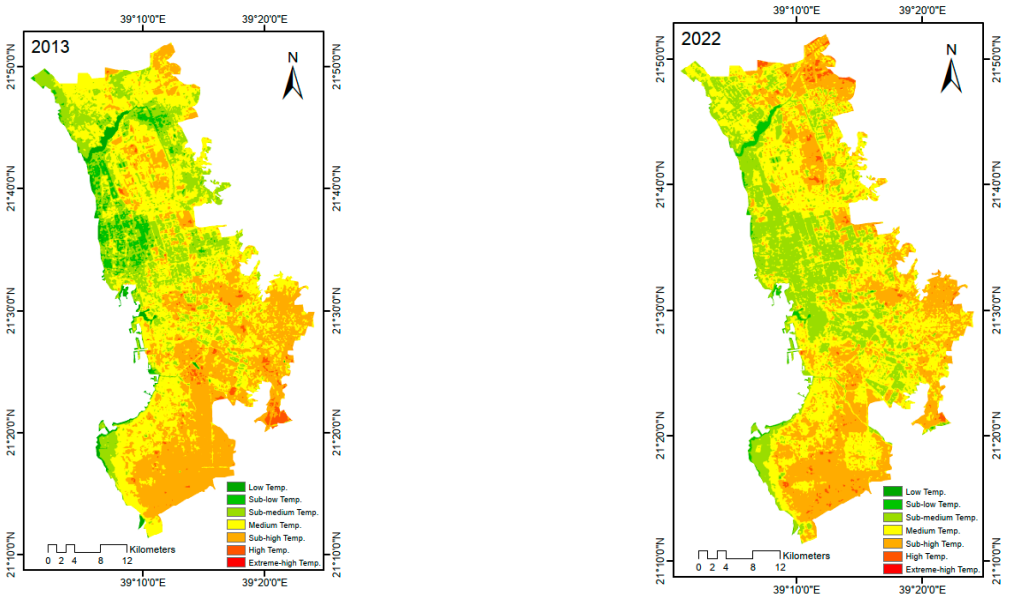


Figure 6. Spatial distribution of LST in Jeddah city, maps from 2013 and 2022.

3.4. LULC Effects on LST

This section aims to analyze the distribution of LST for each LULC class on an annual basis to study the dynamic effect of LULC changes on LST. After calculating the LST in different study years and dividing them into seven interval ranges, the area of each temperature range in the land cover was calculated. Temperature ranges are significant for several reasons, and they can indicate specific environmental conditions and challenges. The higher temperature ranges, particularly the upper extremes, are indicative of areas experiencing the SUHI effect. These ranges can also serve as thresholds for action, both in mitigating the SUHI effect and adapting to changing climate conditions. Table 8 shows the temperature ranges in each year along with the corresponding area within the study area. Then, the changes in LULC during the study period were examined, and the dynamics of the occurring changes in land cover, including their areas and locations, were identified. It has now become necessary to link the changes in LULC with the changes in LST.

As depicted in Figure 4, notable changes are observed primarily in the urban and barren land classes throughout the study period. Consequently, our focus will be directed towards examining the reciprocal changes between these two classes and their correlation with the variations in LST. To do so, the temperature changes from year to year have been determined and divided into the following ranges: ±1 °C, ±2 °C, ±3 °C, ±4 °C, ±5 °C, and 0 indicates that there is no change in LST. Then, the percentage covered by each range was calculated in both cases: the change from urban to barren land and vice versa. Tables 9 and 10 present the percentage of area that has changed from the urban class to the barren land class and vice versa, based on the magnitude of the temperature change. Also, Figure 7 depicts the percentage of changes between urban and barren land classes with respect to the amount of change in LST on an annual basis.

Table 8. LST interval ranges (°C) and corresponding LULC covered area (Km^2).

Interval of LST	2013		2014		2015		2016		2017	
	Range of LST (°C)	Area (km^2)	Range of LST (°C)	Area (km^2)	Range of LST (°C)	Area (km^2)	Range of LST (°C)	Area (km^2)	Range of LST (°C)	Area (km^2)
Low temperature	27.67–36.87	19.61	28.60–38.00	21.75	29.35–39.38	21.75	27.57–35.98	22.98	29.65–38.66	21.03
Sub-low temperature	36.87–38.95	16.07	38.00–40.11	122.22	39.38–41.54	45.02	35.98–37.59	49.04	38.66–40.62	50.60
Sub-medium temperature	38.95–41.02	405.11	40.11–42.22	144.02	41.54–43.70	227.25	37.59–39.21	221.42	40.62–42.59	231.51
Medium temperature	41.02–43.10	497.13	42.22–44.32	571.83	43.70–45.86	555.09	39.21–40.82	532.65	42.59–44.55	537.28
Sub-high temperature	43.10–45.18	238.85	44.32–46.43	342.43	45.86–48.02	344.57	40.82–42.44	380.51	44.55–46.51	369.48
High temperature	45.18–47.25	54.91	46.43–48.54	29.45	48.02–50.18	37.97	42.44–44.05	24.95	46.51–48.47	21.82
Extreme-high temperature	47.25–49.59	0.04	48.54–49.43	0.03	50.18–50.48	0.07	44.05–45.31	0.17	48.47–48.81	0.01
Interval of LST	2018		2019		2020		2021		2022	
	Range of LST (°C)	Area (km^2)	Range of LST (°C)	Area (km^2)	Range of LST (°C)	Area (km^2)	Range of LST (°C)	Area (km^2)	Range of LST (°C)	Area (km^2)
Low temperature	28.73–37.51	20.00	29.07–37.78	21.29	28.94–38.27	20.14	29.34–37.85	20.47	28.77–37.59	19.34
Sub-low temperature	37.51–39.64	54.62	37.78–40.02	59.65	38.27–40.33	48.55	37.85–39.82	54.52	37.59–41.22	294.95
Sub-medium temperature	39.64–41.76	237.92	40.02–42.27	233.00	40.33–42.39	239.82	39.82–41.80	236.11	41.22–43.04	512.83
Medium temperature	41.76–43.89	525.58	42.27–44.51	503.30	42.39–44.45	541.74	41.80–43.77	508.22	43.04–44.85	388.73
Sub-high temperature	43.89–46.02	365.71	44.51–46.76	394.69	44.45–46.51	347.09	43.77–45.75	383.71	44.85–46.66	15.86
High temperature	46.02–48.14	27.83	46.76–49.00	19.77	46.51–48.56	34.34	45.75–47.44	28.68	46.66–46.98	0.00
Extreme-high temperature	48.14–52.2	0.06	49.00–49.38	0.01	48.56–49.81	0.04	47.44–47.52	0.01	46.98–47.05	0.00

Table 9. Percentage (%) of the area that changed from urban to barren land according to the amount of change in temperature.

Period	Temperature Difference										
	(−5) °C	**(−4) °C**	**(−3) °C**	**(−2) °C**	**(−1) °C**	**(0) °C**	**(+1) °C**	**(+2) °C**	**(+3) °C**	**(+4) °C**	**(+5) °C**
2013–2014	0.05	0.13	0.39	1.19	9.80	27.46	19.70	19.38	14.66	6.60	0.64
2014–2015	0.00	0.00	0.01	0.05	0.80	9.48	28.43	46.00	12.77	1.63	0.81
2015–2016	13.98	46.31	29.00	9.69	0.92	0.07	0.02	0.01	0.00	0.00	0.00
2016–2017	0.00	0.00	0.00	0.01	0.01	0.67	5.33	37.72	37.82	13.25	5.19
2017–2018	0.03	0.15	1.28	11.85	45.14	39.73	1.68	0.08	0.04	0.01	0.01
2018–2019	0.00	0.01	0.04	0.26	8.36	35.72	43.90	10.69	0.93	0.07	0.04
2019–2020	0.00	0.00	0.23	2.89	15.78	37.92	38.04	4.60	0.40	0.11	0.03
2020–2021	0.04	0.13	0.54	11.03	26.95	18.55	30.88	11.14	0.55	0.14	0.05
2021–2022	0.00	0.07	0.47	6.77	31.65	16.43	36.72	7.23	0.57	0.08	0.01

Table 10. Percentage (%) of the area changed from barren land to urban according to the amount of change in temperature.

Period	Temperature Difference										
	(−5) °C	**(−4) °C**	**(−5) °C**	**(−2) °C**	**(−5) °C**	**(0) °C**	**(−5) °C**	**(+2) °C**	**(−5) °C**	**(+4) °C**	**(−5) °C**
2013–2014	0.08	0.32	0.72	1.82	10.76	22.62	20.21	23.23	14.62	4.81	0.81
2014–2015	0.00	0.01	0.04	0.17	1.21	10.68	32.47	41.54	11.50	1.49	0.88
2015–2016	14.96	38.61	32.15	13.19	1.04	0.03	0.01	0.00	0.00	0.00	0.00
2016–2017	0.01	0.02	0.04	0.06	0.17	1.69	10.59	31.07	32.89	16.13	7.34
2017–2018	0.06	0.17	1.54	10.96	46.98	38.76	1.47	0.05	0.00	0.00	0.00
2018–2019	0.02	0.02	0.09	0.42	9.29	35.88	41.77	11.15	1.24	0.10	0.03
2019–2020	0.01	0.03	0.47	3.20	16.62	36.42	38.40	4.28	0.52	0.05	0.01
2020–2021	0.07	0.17	0.59	8.41	27.26	22.64	31.41	8.61	0.59	0.18	0.07
2021–2022	0.02	0.05	0.34	6.18	34.12	14.73	37.55	6.55	0.39	0.05	0.02

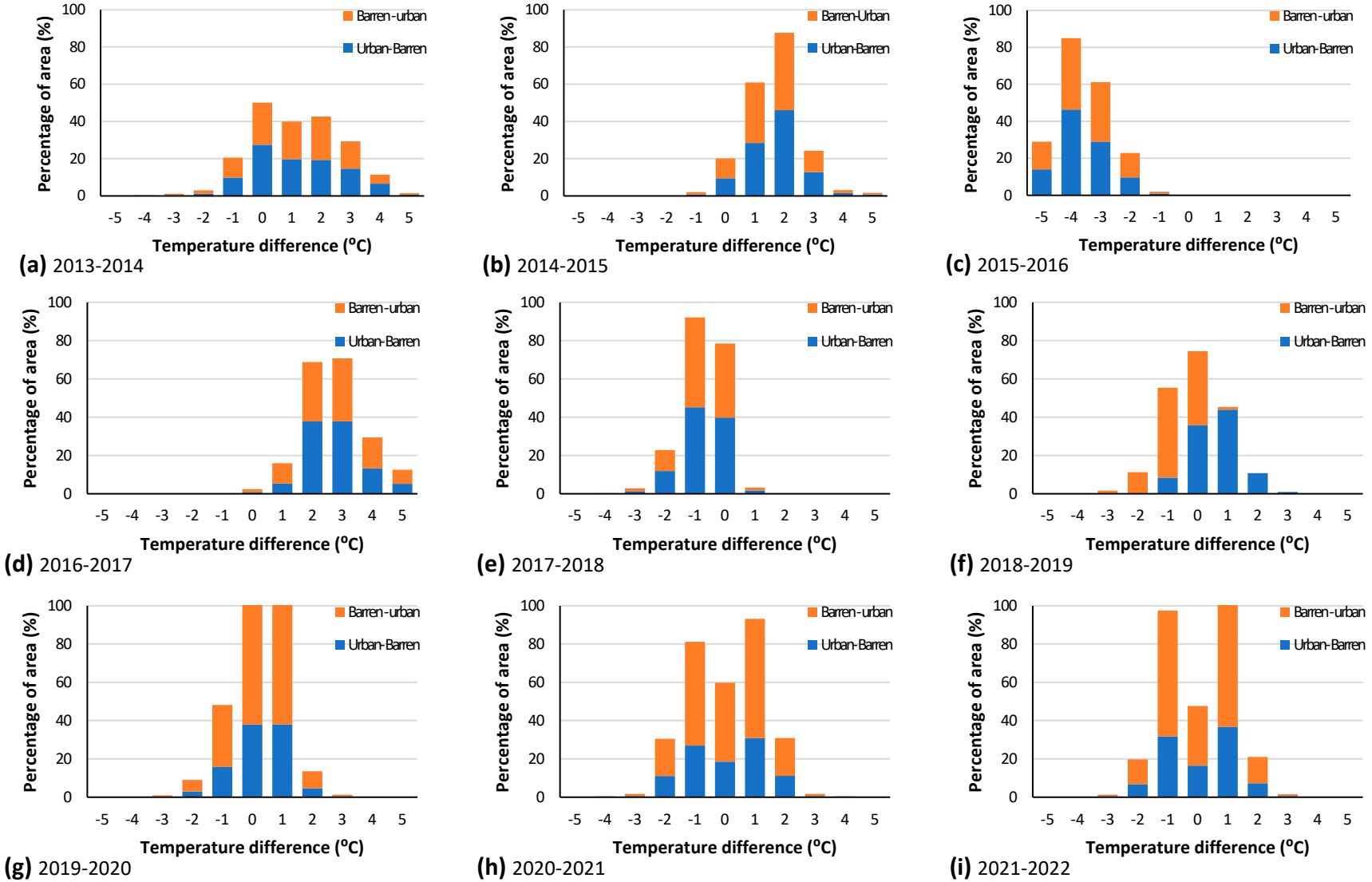
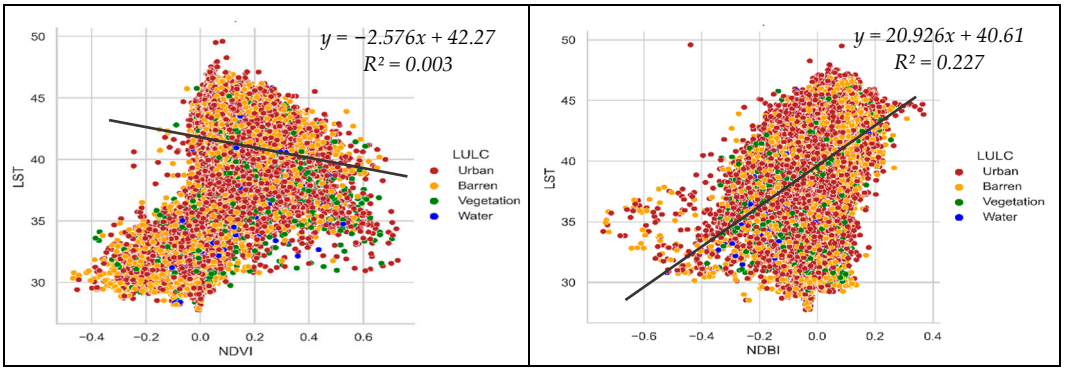


Figure 7. Percentage (%) of the area that changed according to the amount of change in temperature between urban and barren land.

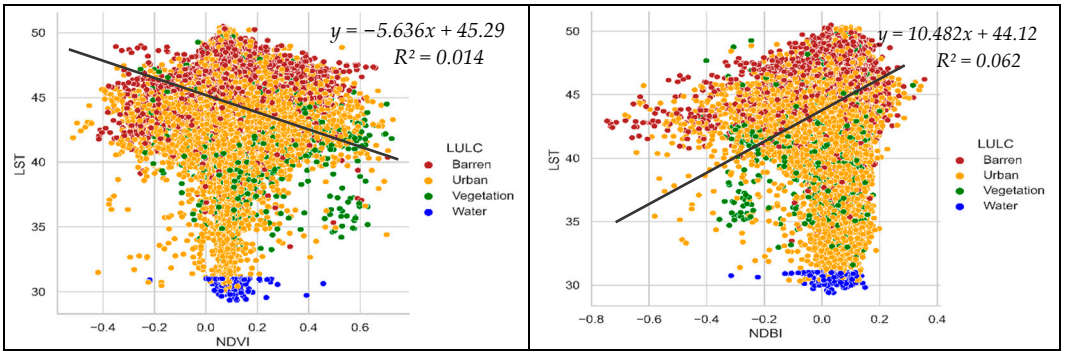
The spatiotemporal maps of NDVI and NDBI indices for the study area were derived from satellite images for specific time-points: 2013, 2015, 2017, and 2022. This selection was based on the observation that a significant increase in the mean LST of most classes began in 2013 and continued until 2015, followed by a decrease from 2017 until 2022. These indices were then correlated with LST through scatter plots. The results, shown in Figure 8, indicate a negative correlation between LST and NDVI values, and a positive relationship between LST and NDBI values for all selected years. So, it can be stated that LST increased due to the presence of lower vegetation. On the other hand, an increase in high-density built-up areas leads to an increase in LST values. The negative correlation between LST and NDVI signifies the inverse relationship between temperature and vegetation. Healthy vegetation transpires water and provides shade, reducing the amount of solar energy absorbed and, consequently, lowering the LST. While the positive relationship between LST and NDBI is due to the fact that urban areas have a higher percentage of impervious surfaces such as buildings and roads. These surfaces absorb and retain heat from the sun, causing them to become much hotter. Recognizing these relationships is essential for urban planners in Jeddah who aim to mitigate urban heat islands through strategies like increasing green spaces and designing energy-efficient buildings.

3.5. SUHIs Delineation

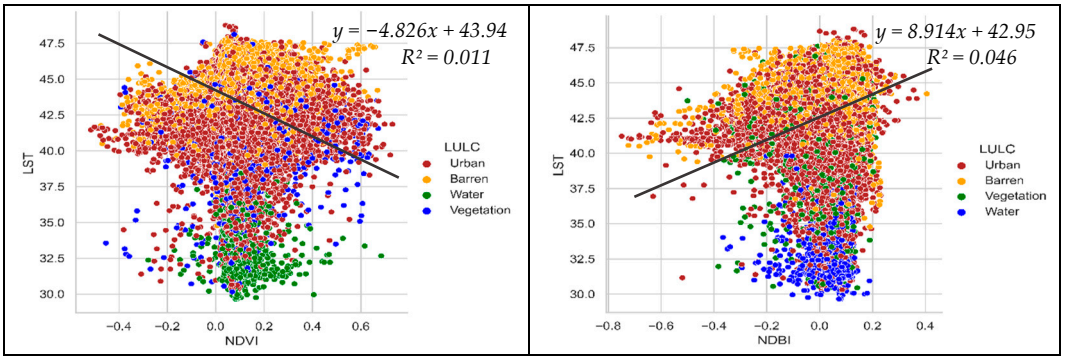
As mentioned in the introduction, this study aims to determine the impact of LULC on the increase in LST and the formation of SUHIs during the study period. The focus was not on evaluating the heat islands, but rather on their presence or absence. After estimating the LST and categorizing them into classes as shown in Table 2, it was considered that places with extreme-high temperature surrounded by sub-high or medium temperature are centers of SUHIs. These centers were identified and mapped in each year of the study, considering a coverage area with a radius of 5 km as a range of the heat island's influence. Figure 9 shows the distribution of heat islands in Jeddah city from 2013 to 2022. Furthermore, the results of the URI calculations are displayed in Figure 10. The URI graph demonstrates that the intensity of SUHI increased from 0.16 in 2013 to 0.22 in 2014. From 2014 to 2021, the URI value fluctuated between 0.2 and 0.25, reaching a maximum value of 0.24 in 2016. However, in 2022, the value decreased dramatically to 0.12.



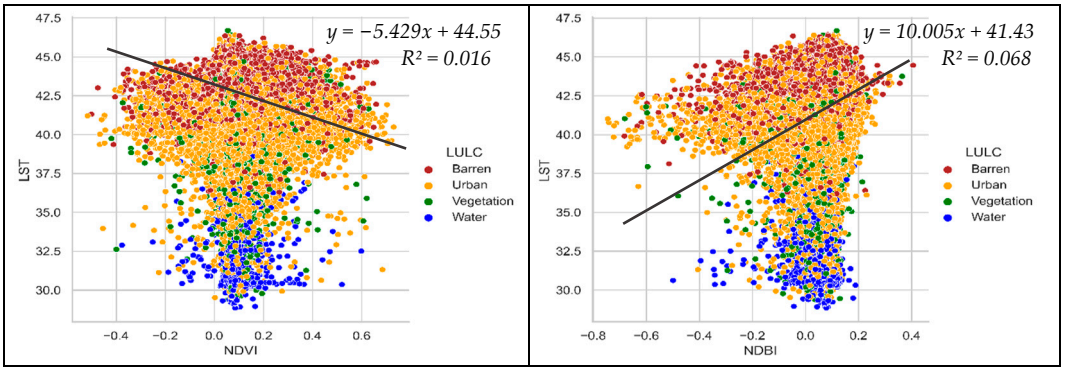
2013



2015



2017



2022

Figure 8. Relationship between LST with NDVI and NDBI for selected years of the study area.

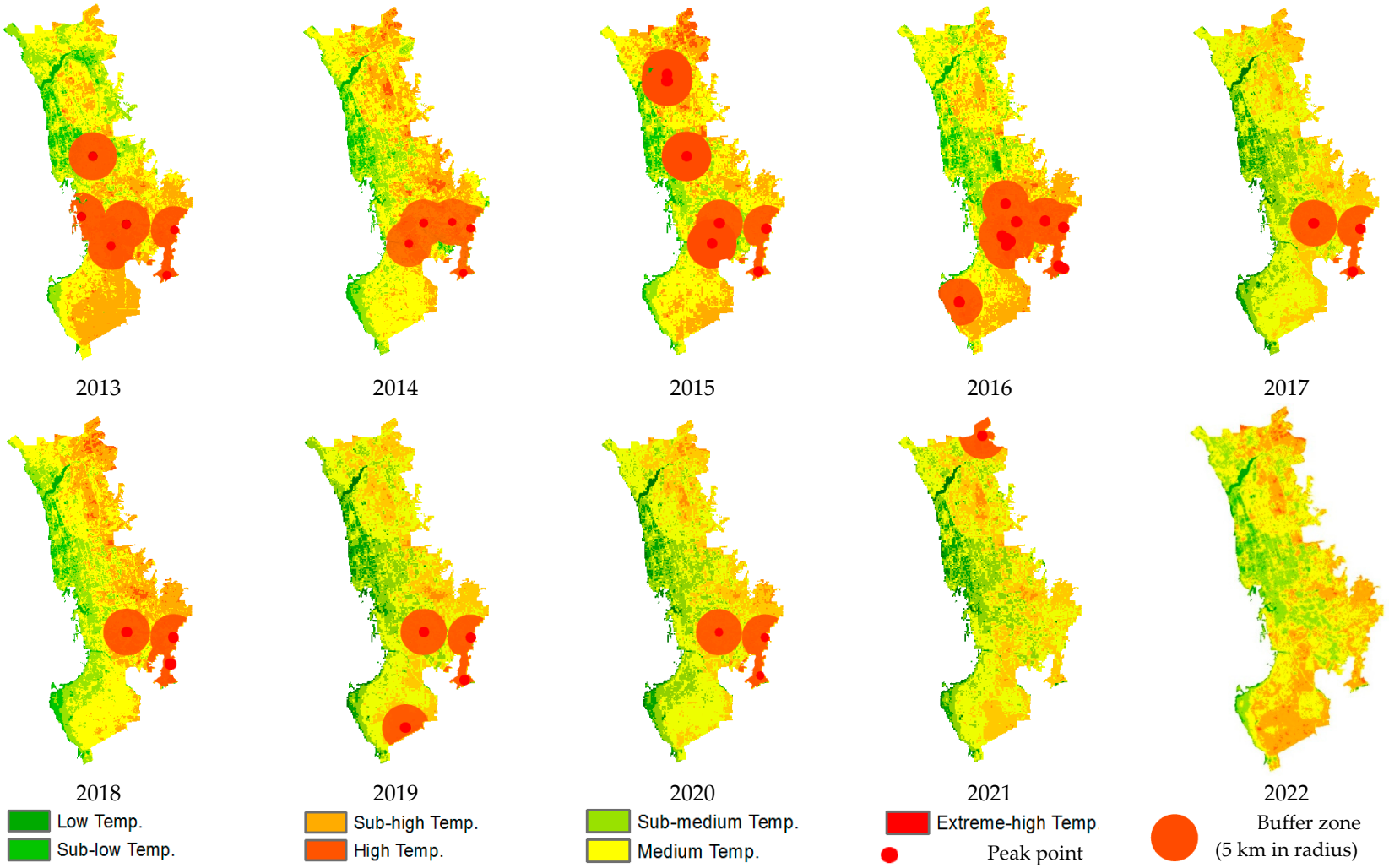


Figure 9. Mapping of SUHIs in Jeddah city from 2013 to 2022.

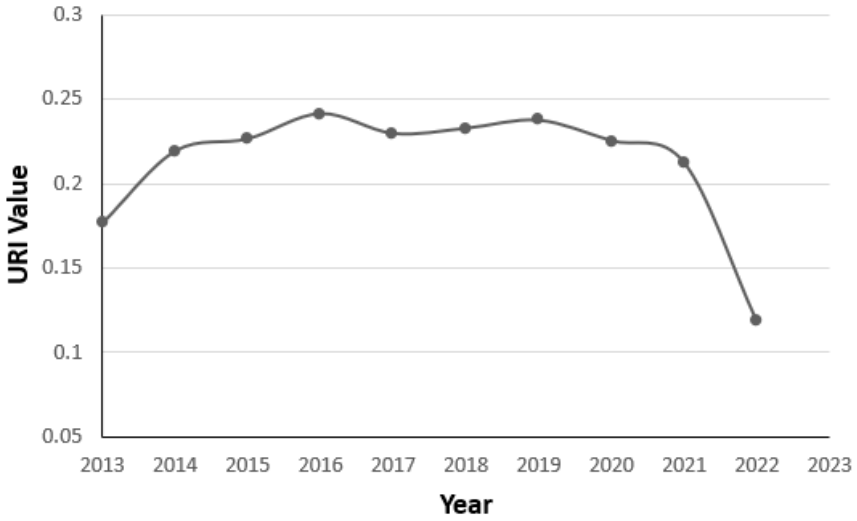


Figure 10. Urban heat island ratio index (URI) for the study area from 2013 to 2022.

4. Discussion

4.1. Analysis of the Urban Development Strategies

To improve the quality of life in Jeddah city and to achieve high-quality urbanization trends, a comprehensive development process was initiated in the last years. This, based on the change detection results, may have contributed remarkably to the transition of built areas into barren lands as a first step before installing new urban planning. As mentioned in the introduction to the study, the new urban planning includes developing infrastructure and services and creating new projects to improve the quality of life in accordance with the Kingdom's 2030 vision [35]. The first step involves the elimination of certain old, illegal districts in Jeddah, about 34 neighborhoods in different areas were removed [36], which appeared in the results of change detection. This results in alterations to the land cover characteristics. Since SUHIs are sensitive to explicit factors of LULC and urban development [5], these modifications subsequently affect the thermal energy balance and are leading to shifts in the local climate, which is represented by a local increase in LST [31]. Therefore, the main objective of this study was to track the dynamics of LULC changes and associated urban development strategies and their influence on LST within the city of Jeddah.

4.2. Land Use and Land Cover Changes

In today's era of big data, the availability of advanced robust techniques and cloud computing platforms has made large-scale analysis possible at a low cost [34,45]. Thanks to Google Earth Engine (GEE), about 40 different scenes from the Landsat satellite were remotely accessed and classified. Additionally, all the required indices were easily calculated using automatic parallel processing and robust computational abilities provided by GEE. The overall accuracy, using reference data validated by Google Earth, exceeded 95% for all performed classifications.

The heterogeneous spatiotemporal LULC changes from 2013 to 2022 have shown both negative and positive changes in the various LULC classes. Water bodies and vegetation cover, as blue–green spaces, hold significant implications in urban development. However, the percentage of vegetation cover and water bodies in the study area decreased following the commencement of the demolishing project. Remarkably, LST also decreased during this period, suggesting that the influence of these blue–green spaces on LST was minimal. As mentioned earlier, the changes in water and vegetation classes were negligible due to the lower presence of those classes in this arid region. Changes from urban to barren land is attributed to the comprehensive development project in Jeddah to improve the quality of life aligning with the Kingdom's 2030 vision. Even though, 34 neighborhoods in various regions have been demolished [36], the results of the change detection indicate that the total urban

areas in the study area have increased compared to the total barren land areas from 2013 to 2022. This change from barren land to urban can be attributed to the efforts of the government in providing alternative housing projects for the residents of the demolished neighborhoods through the creation of new urban areas according to a well-planned urban design.

4.3. Impact on LST55

The rise in LST caused by LULC is a widespread phenomenon that occurs all over the world [30–33]. A variety of external factors such as latitude, soil type, weather conditions etc. play a big role in determining the degree of change [34]. In our case, the situation is different for several reasons. Firstly, the study area is arid, so the impact of increased vegetation cover on reducing LST rise is almost nonexistent due to the scarcity of plants in this environment. The percentage of vegetation cover was 4.34% in 2013, 5.33% in 2022, and reached its highest value of 5.51% in 2014. Secondly, the comprehensive development process project, which began the removal of old informal and illegal settlements from the city center, had a significant influence on LST changes. We found that the mean LST began to noticeably decrease starting from 2020 when the project commenced. Thirdly, the geographical location of Jeddah is significant. It extends longitudinally along the Red Sea coast, without a centralized urban area in the city. The presence of the sea acts as a natural cooling mechanism and significantly influences LST. Coastal areas benefit from cooling breezes resulting from the temperature differential between the land and sea. These breezes have a pronounced effect on reducing LST along the coastline, making these regions notably cooler than inland areas. As demonstrated in Figure 11, the temperature gradients along the cross-sectional profiles A, B, and C illustrate this phenomenon. LST begins at lower values in the coastal area and gradually increases, typically reaching its highest values farther from the sea.

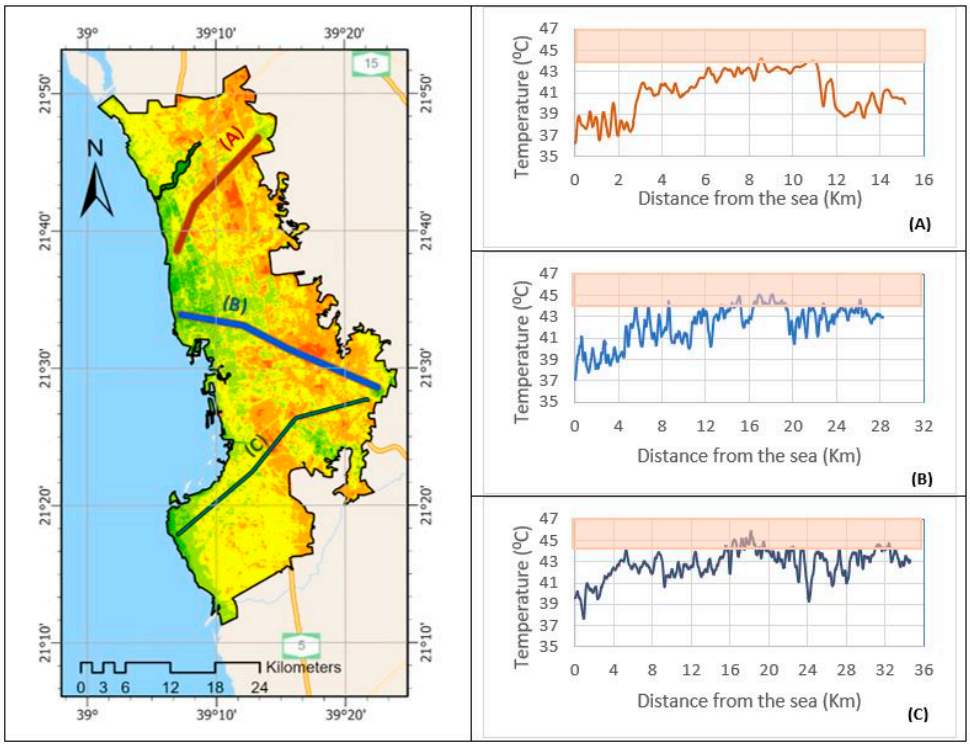


Figure 11. LST gradients along the cross-sectional profiles A, B, and C for the year 2013.

It is clear from the results that LST values varied according to land use and the increase in heterogeneity in land cover features. During the study periods between 2013 and 2022, the barren lands have recorded the most mean LST, followed by the built-up

areas, vegetation, and water bodies. While, for maximum LST recorded, the built-up areas have recorded maximum LST, followed by barren lands, vegetation, and water bodies.

The results of the study revealed a clear inverse linear correlation between LST and NDVI throughout the study duration. This indicates that the reduction in vegetation cover significantly contributed to the rise in LST. Moreover, a positive correlation was observed between LST and NDBI, signifying that an expansion of built-up areas leads to an escalation in LST. These outcomes align with results from comparable studies that relied on Landsat data analysis [52,53,58–60].

4.4. Spatial Analysis of SUHIs

The classification of LST into various classes allowed for the identification of areas with extreme-high temperatures surrounded by sub-high or medium temperatures, which were considered as centers of SUHIs. These centers were tracked and mapped over the years. This provides a comprehensive view of the spatiotemporal dynamics of SUHIs. According to previous studies, heat islands in Jeddah are predominantly concentrated in the southern region [3]. These areas mostly consist of informal and industrial regions that have been recently removed. Figure 9 visually illustrates the distribution of these heat islands in Jeddah City from 2013 to 2022. It is apparent from the map that the presence and intensity of SUHIs vary across different years, indicating the dynamic nature of SUHIs in the city. The concentration of UHIs was in the southern part and the middle of the city until 2016, after that the concentration of UHIs decreased. In 2022, complete absence of the SUHIs over the city was noticed. The disappearance of SUHIs can result from various factors, including urban planning, climate change, or mitigation efforts. In our study, it was due to implementation of the new urban development strategy and demolition of old districts. This has a significant positive implication on human thermal comfort, urban heat management, and energy savings.

4.5. Limitations

There are some limitations to this study. First, regarding the data used, on the one hand, The image spatial resolution was 30 m, and this caused inaccuracies in linking the estimated LST with the LULC, especially for the small blocks. On the other hand, the availability of cloud-free data, which is essential to calculate accurate LST, for the required time-points is a major limitation of this study.

In this study, we focus on land use changes as the only factors influencing LST changes. It is important to note that other variables, such as weather changes over the study period, may also impact LST. Future research could yield more insights by extending the study period beyond just the summer months and considering weather variations throughout the year.

5. Conclusions

This study provides a comprehensive assessment of SUHIs in Jeddah City based on LST during a 10-year period (2013–2022), shedding light on their presence, and temporal variations. The spatiotemporal pattern of LULC changes was configured for different time-points and four different LULC classes including: urban, vegetation, barren lands, and water bodies. Average summer LST was calculated, and the variation of LST with NDVI, and NDBI was assessed. Additionally, URI was used to illustrate the variation of the intensity of SUHI in the study area. The results showed notable heterogeneous spatiotemporal LULC changes showing both negative and positive changes in the various LULC classes spatially between urban and barren land classes. Through an examination of the LST distribution pattern and the mapping of SUHIs in Jeddah city over the study duration, it becomes evident that a substantial direct correlation exists between the density of built-up areas and LST. Furthermore, the findings highlight a significant negative association between LST and the NDVI, whereas a positive correlation was consistently observed between LST and NDBI across all time points. From the calculation of the URI,

it is seen that the value of URI reached its maximum of 0.24 in 2016 with the presence of SUHIs, then it decreased dramatically to reach 0.12 in 2022 with an absence of SUHI. It was evident that the complete absence of SUHI in 2022 was due to the removal of old informal and illegal settlements from the city. The findings have implications for urban planning, climate adaptation, and further research into the underlying causes of these urban heat phenomena. Understanding and addressing SUHIs is crucial for creating more sustainable and livable urban environments.

Author Contributions: Conceptualization, Y.M.; Data curation, Y.M.; Formal analysis, Y.M.; Funding acquisition, Y.M.; Investigation, Y.M., A.A.S. and A.A.; Methodology, Y.M. and A.A.; Project administration, Y.M.; Resources, Y.M., A.A.S. and A.A.; Software, Y.M. and A.A.S.; Supervision, Y.M.; Validation, Y.M., A.A.S. and A.A.; Visualization, Y.M.; Writing—original draft, Y.M. and A.A.S.; Writing—review and editing, A.A. All authors have read and agreed to the published version of the manuscript.

Funding: The Deanship of Scientific Research (DSR) at King Abdulaziz University (KAU), Jeddah, Saudi Arabia has funded this project, under grant number (G: 459-137-1443).

Institutional Review Board Statement: Not applicable.

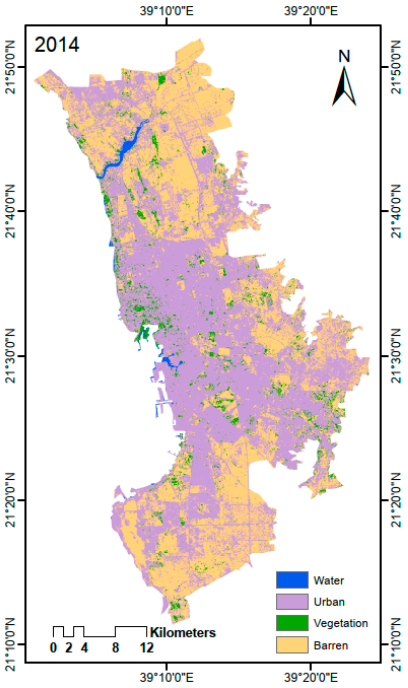
Informed Consent Statement: Not applicable.

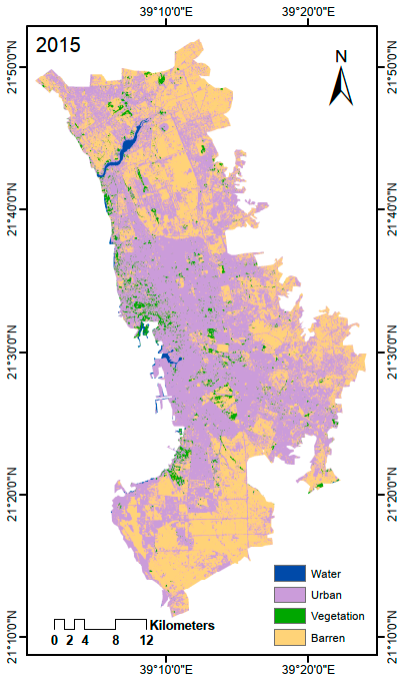
Data Availability Statement: The data that support the findings of this study are available on request from the corresponding author.

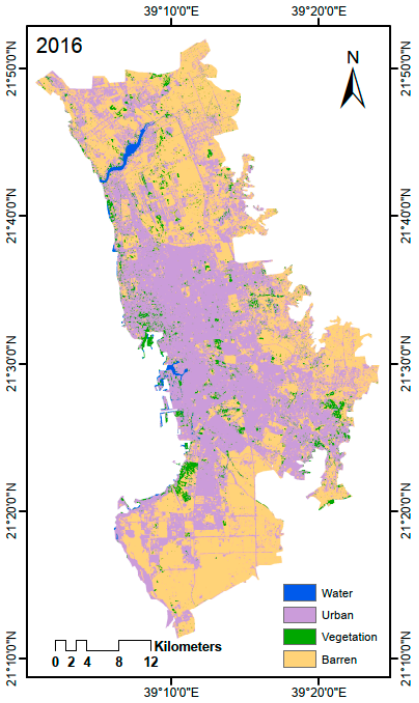
Acknowledgments: The authors gratefully acknowledge the technical and financial support provided by the Deanship of Scientific Research at King Abdulaziz University, Jeddah, Saudi Arabia.

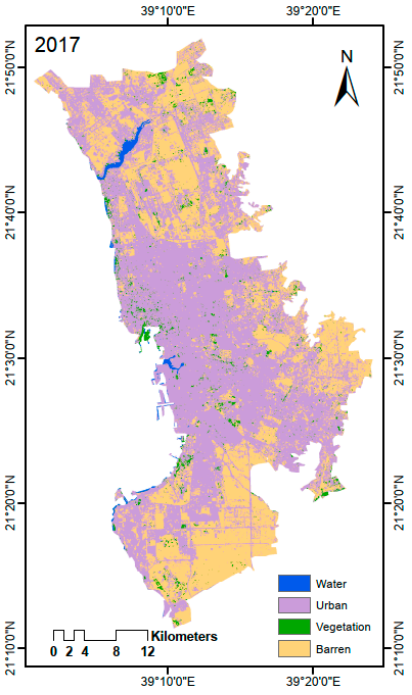
Conflicts of Interest: The authors declare no conflict of interest.

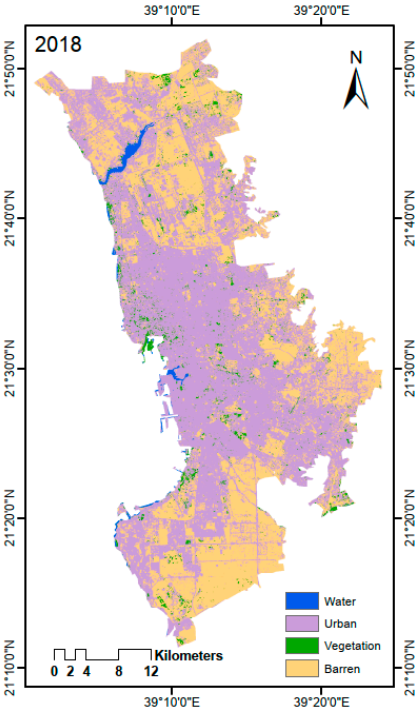
Appendix A. Spatial LULC in Jeddah City, from 2014 to 2021

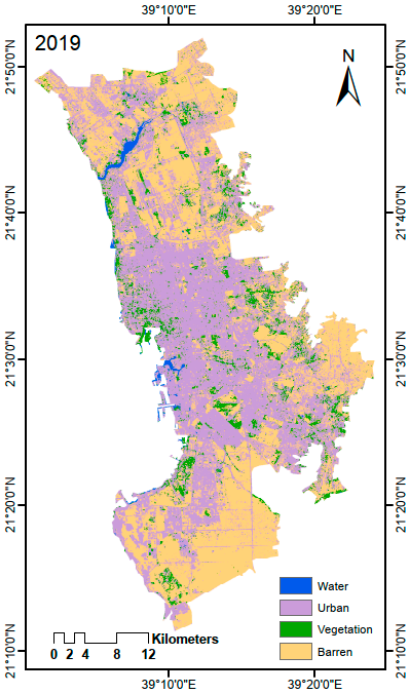


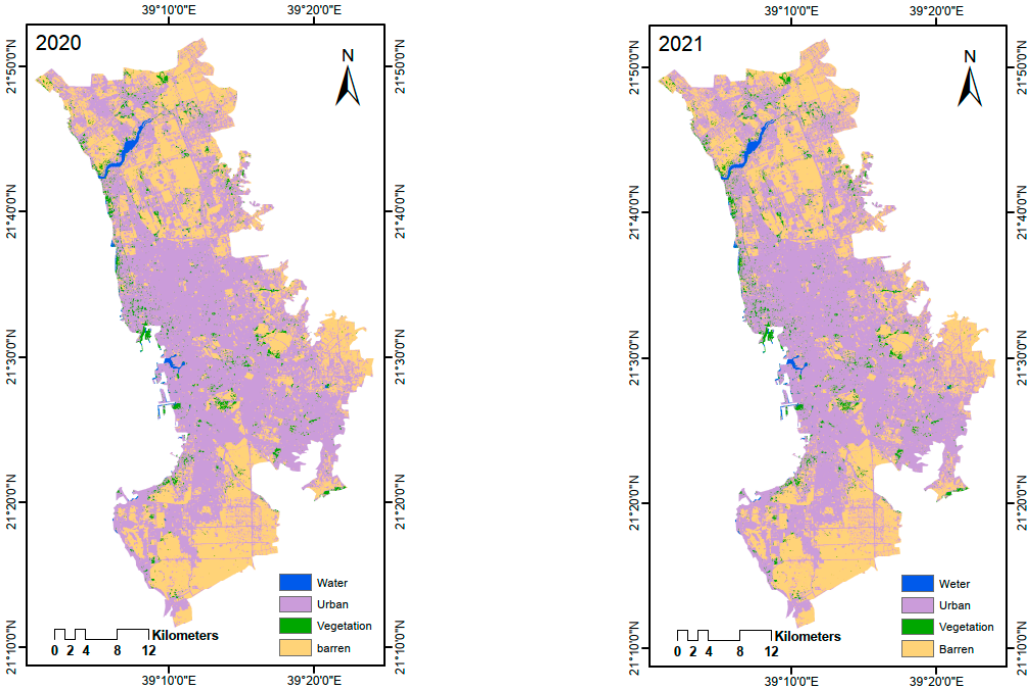



2016
N
39°10'0"E
39°20'0"E
21°50'0"N
21°40'0"N
21°30'0"N
21°20'0"N
21°10'0"N
Water
Urban
Vegetation
Barren
Kilometers
0 2 4 8 12

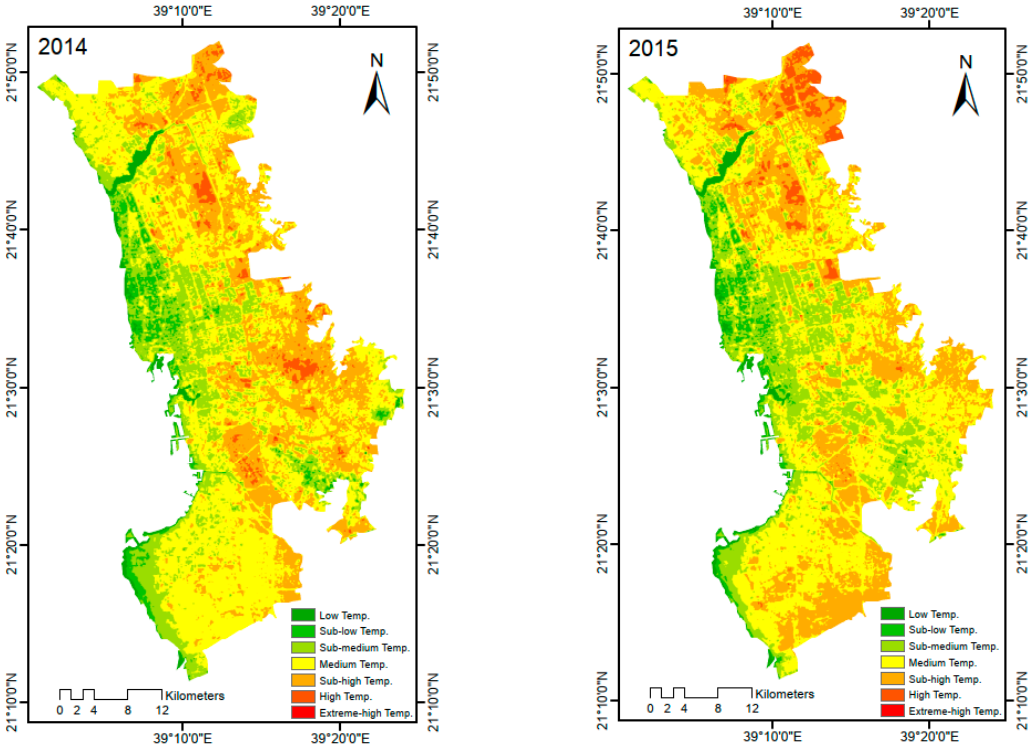

2017
N
39°10'0"E
39°20'0"E
21°50'0"N
21°40'0"N
21°30'0"N
21°20'0"N
21°10'0"N
Water
Urban
Vegetation
Barren
Kilometers
0 2 4 8 12

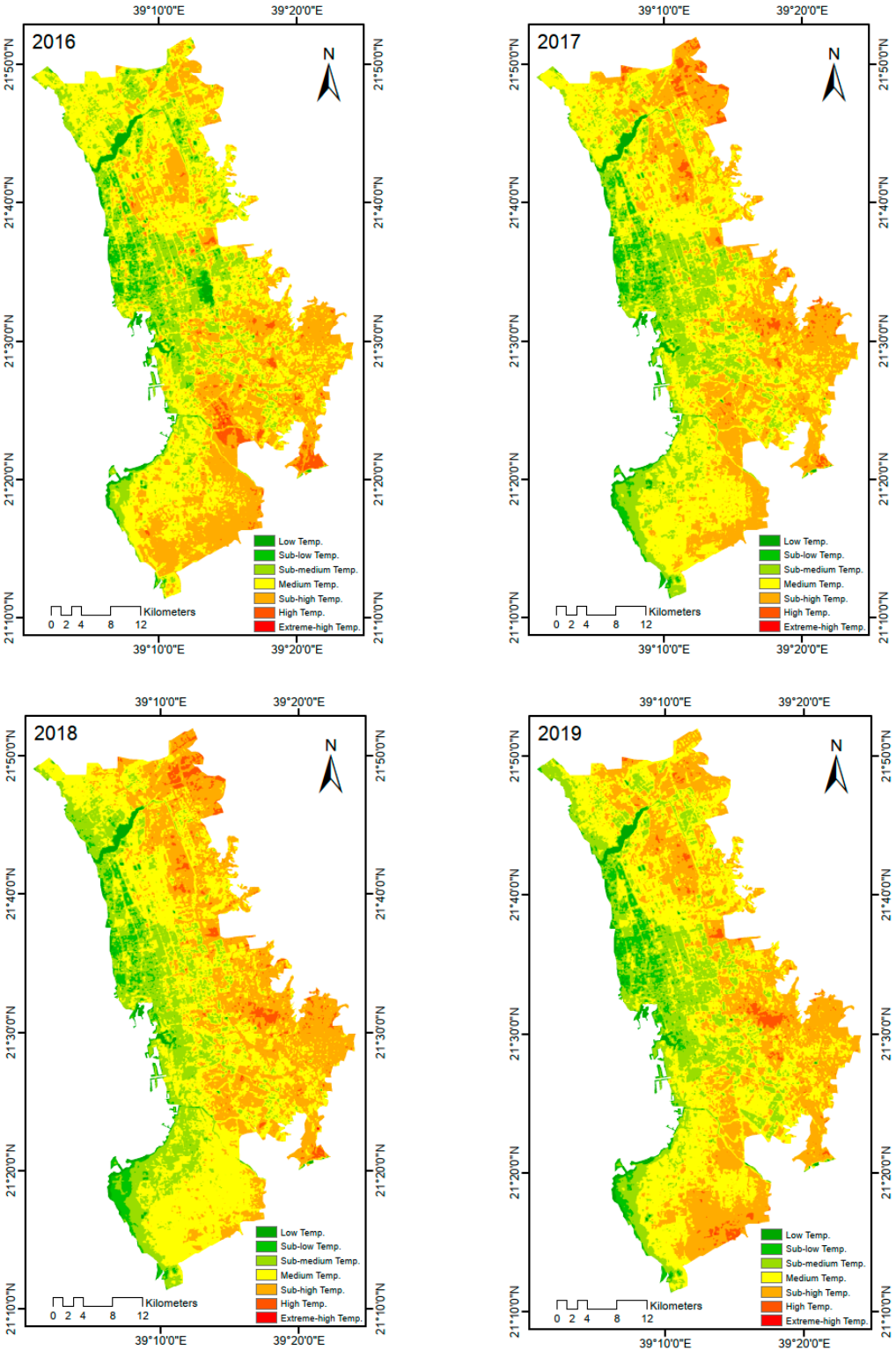

2018
N
39°10'0"E
39°20'0"E
21°50'0"N
21°40'0"N
21°30'0"N
21°20'0"N
21°10'0"N
Water
Urban
Vegetation
Barren
Kilometers
0 2 4 8 12

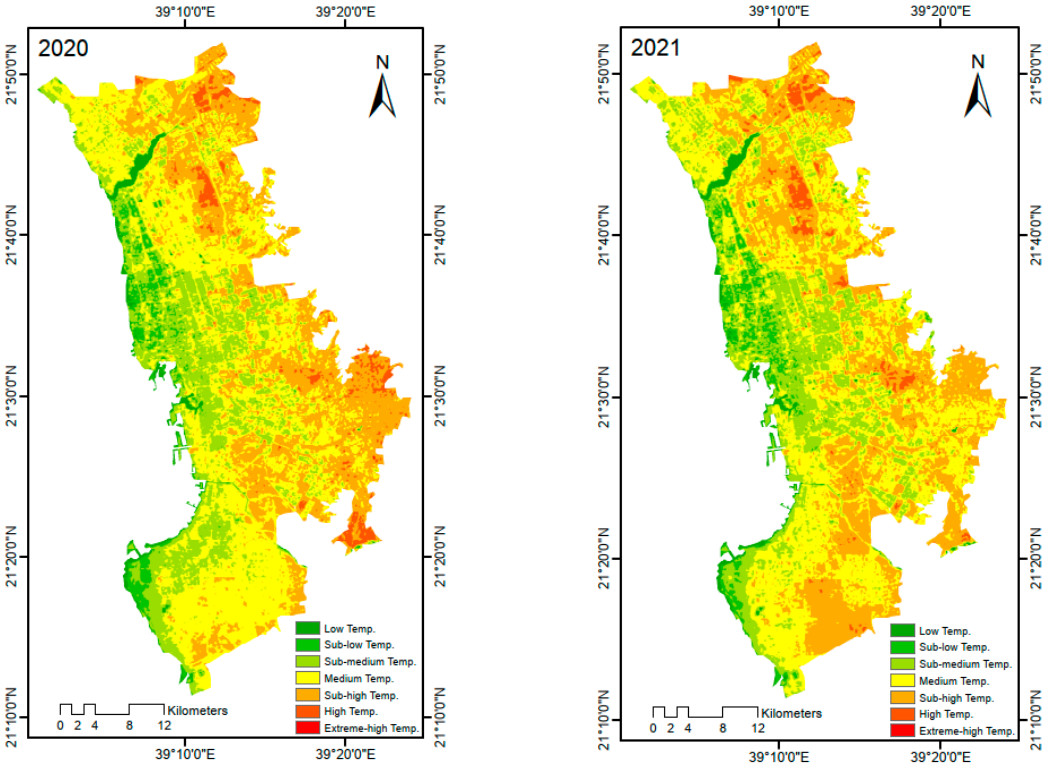

2019
N
39°10'0"E
39°20'0"E
21°50'0"N
21°40'0"N
21°30'0"N
21°20'0"N
21°10'0"N
Water
Urban
Vegetation
Barren
Kilometers
0 2 4 8 12



Appendix B. Spatial Distribution of LST in Jeddah City, form 2014 to 2021




2016
2017
2018
2019
N
39°10'0"E
39°20'0"E
21°50'0"N
21°40'0"N
21°30'0"N
21°20'0"N
21°10'0"N
Low Temp.
Sub-low Temp.
Sub-medium Temp.
Medium Temp.
Sub-high Temp.
High Temp.
Extreme-high Temp.
Kilometers
0 2 4 8 12



References

1. Lu, D.; Song, K.; Zang, S.; Jia, M.; Du, J.; Ren, C. The effect of urban expansion on urban surface temperature in Shenyang, China: An analysis with Landsat imagery. *Environ. Model. Assess.* **2015**, *20*, 197–210. [CrossRef]
2. Silva, J.S.; da Silva, R.M.; Santos, C.A.G. Spatiotemporal impact of land use/land cover changes on urban heat islands: A case study of Paço do Lumiar, Brazil. In *Building and Environment*; Elsevier: Amsterdam, The Netherlands, 2018; Volume 136, pp. 279–292. [CrossRef]
3. Miky, Y.H. Remote sensing analysis for surface urban heat island detection over Jeddah, Saudi Arabia. *Appl. Geomat.* **2019**, *11*, 243–258. [CrossRef]
4. Simperler, L.; Ertl, T.; Matzinger, A. Spatial Compatibility of Implementing Nature-Based Solutions for Reducing Urban Heat Islands and Stormwater Pollution. *Sustainability* **2020**, *12*, 5967. [CrossRef]
5. He, B.-J.; Wang, J.; Liu, H.; Ulpiani, G. Localized synergies between heat waves and urban heat islands: Implications on human thermal comfort and urban heat management. *Environ. Res.* **2021**, *193*, 110584. [CrossRef] [PubMed]
6. Oke, T.R.; Mills, G.; Christen, A.; Voogt, J.A. *Urban Clim.*; Cambridge University Press: Cambridge, UK, 2017.
7. He, B.-J.; Zhao, Z.-Q.; Shen, L.-D.; Wang, H.-B.; Li, L.-G. An approach to examining performances of cool/hot sources in mitigating/enhancing land surface temperature under different temperature backgrounds based on Landsat 8 image. *Sustain. Cities Soc.* **2019**, *44*, 416–427. [CrossRef]
8. Guo, A.; Yang, J.; Sun, W.; Xiao, X.; Xia Cecilia, J.; Jin, C.; Li, X. Impact of urban morphology and landscape characteristics on spatiotemporal heterogeneity of land surface temperature. *Sustain. Cities Soc.* **2020**, *63*, 102443. [CrossRef]
9. Lemonsu, A.; Viguie, V.; Daniel, M.; Masson, V. Vulnerability to heat waves: Impact of urban expansion scenarios on urban heat island and heat stress in Paris (France). *Urban Clim.* **2015**, *14*, 586–605. [CrossRef]
10. Ozawa-Meida, L.; Ortiz-Moya, F.; Painter, B.; Hengesbaugh, M.; Nakano, R.; Yoshida, T.; Zusman, E.; Bhattacharyya, S. Integrating the Sustainable Development Goals (SDGs) into Urban Climate Plans in the UK and Japan: A Text Analysis. *Climate* **2021**, *9*, 100. [CrossRef]
11. Tang, K.; Zhu, H.; Ni, P. Spatial Downscaling of Land Surface Temperature over Heterogeneous Regions Using Random Forest Regression Considering Spatial Features. *Remote Sens.* **2021**, *13*, 3645. [CrossRef]
12. Parastatidis, D.; Mitraka, Z.; Chrysoulakis, N.; Abrams, M. Online Global Land Surface Temperature Estimation from Landsat. *Remote Sens.* **2017**, *9*, 1208. [CrossRef]
13. Quattrochi, D.A.; Luvall, J.C. Thermal Infrared Remote Sensing for Analysis of Landscape Ecological Processes: Methods and Applications. *Landsc. Ecol.* **1999**, *14*, 577–598. [CrossRef]
14. Wu, X.; Wang, G.; Yao, R.; Wang, L.; Yu, D.; Gui, X. Investigating Surface Urban Heat Islands in South America Based on MODIS Data from 2003–2016. *Remote Sens.* **2019**, *11*, 1212. [CrossRef]

15. Koko, A.F.; Yue, W.; Abubakar, G.A.; Alabsi, A.A.N.; Hamed, R. Spatiotemporal Influence of Land Use/Land Cover Change Dynamics on Surface Urban Heat Island: A Case Study of Abuja Metropolis, Nigeria. *ISPRS Int. J. Geo-Inf.* **2021**, *10*, 272. [CrossRef]
16. Reid, R.S.; Kruska, R.L.; Muthui, N.; Taye, A.; Wotton, S.; Wilson, C.J.; Mulatu, W. Land-use and land-cover dynamics in response to changes in climatic, biological and socio-political forces: The case of southwestern Ethiopia. *Landsc. Ecol.* **2000**, *15*, 339–355. [CrossRef]
17. Wang, H.; Zhang, Y.; Tsou, J.Y.; Li, Y. Surface Urban Heat Island Analysis of Shanghai (China) Based on the Change of Land Use and Land Cover. *Sustainability* **2017**, *9*, 1538. [CrossRef]
18. Alexander, P.J.; Mills, G. Local Climate Classification and Dublin's Urban Heat Island. *Atmosphere* **2004**, *5*, 755–774. [CrossRef]
19. Abuloye, A.P.; Popoola, K.S.; Adewale, A.O.; Onana, V.E.; Elugoke, N.O. Assessment of Daytime Surface Urban Heat Island in Onitsha, Nigeria. In Proceedings of the 2015 International Conference and 29th Annual General Meeting of the Nigerian Meteorological Society, Sokoto, Nigeria, 23–26 November 2015.
20. Palafox-Juárez, E.B.; López-Martínez, J.O.; Hernández-Stefanoni, J.L.; Hernández-Nuñez, H. Impact Urban Land-Cover Changes Spat. -Temporal Land Surf. Temp. A Trop. City Mexico. *ISPRS Int. J. Geo-Inf.* **2021**, *10*, 76. [CrossRef]
21. Barbosa, G.S.; Drach, P.R.C.; Corbella, O.D. Intraurban Temperature Variations: Urban Morphologies of the Densification Process of Copacabana Neighborhood, Brazil. *Climate* **2019**, *7*, 65. [CrossRef]
22. Palme, M.; Lobato, A.; Carrasco, C. Quantitative Analysis of Factors Contributing to Urban Heat Island Effect in Cities of Latin-American Pacific Coast. *Procedia Eng.* **2016**, *169*, 199–206. [CrossRef]
23. Bokaie, M.; Zarkesh, M.K.; Arasteh, P.D.; Hosseini, A. Assessment of Urban Heat Island Based on the Relationship Between Land Surface Temperature and Land Use/Land Cover in Tehran. *Sustain. Cities Soc.* **2016**, *23*, 94–104. [CrossRef]
24. Chen, Y.C.; Hao, W.C.; Yuan, F.S.; Yii, C.W.; Ke, S.C. Does Urbanization Increase Diurnal Land Surface Temperature Variation? Evidence and Implications. *Landsc. Urban Plan.* **2017**, *157*, 247–258. [CrossRef]
25. Dissanayake, D.M.S.L.B.; Morimoto, T.; Ranagalage, M.; Murayama, Y. Land-Use/Land-Cover Changes and Their Impact on Surface Urban Heat Islands: Case Study of Kandy City, Sri Lanka. *Climate* **2019**, *7*, 99. [CrossRef]
26. Sultana, S.; Satyanarayana, A.N.V. Assessment of Urbanisation and Urban Heat Island Intensities Using Landsat Imageries During 2000–2018 Over a Sub-Tropical Indian City. *Sustain. Cities Soc.* **2020**, *52*, 101846. [CrossRef]
27. Xiao, H.; Kopecká, M.; Guo, S.; Guan, Y.; Cai, D.; Zhang, C.; Zhang, X.; Yao, W. Responses of Urban Land Surface Temperature on Land Cover: A Comparative Study of Vienna and Madrid. *Sustainability* **2018**, *10*, 260. [CrossRef]
28. Chi, Q.; Zhou, S.; Wang, L.; Zhu, M.; Liu, D.; Tang, W.; Zhao, X.; Xu, S.; Ye, S.; Lee, J.; et al. Quantifying the Contribution of LUCC to Surface Energy Budget: A Case Study of Four Typical Cities in the Yellow River Basin in China. *Atmosphere* **2021**, *12*, 1374. [CrossRef]
29. Jiang, J.; Zhou, Y.; Guo, X.; Qu, T. Calculation and Expression of the Urban Heat Island Indices Based on GeoSOPT Grid. *Sustainability* **2022**, *14*, 2588. [CrossRef]
30. Espinoza-Molina, J.; Acosta-Caipa, K.; Chambe-Vega, E.; Huayna, G.; Pino-Vargas, E.; Abad, J. Spatiotemporal Analysis of Urban Heat Islands in Relation to Urban Development, in the Vicinity of the Atacama Desert. *Climate* **2022**, *10*, 87. [CrossRef]
31. Mohamed, M.A. Spatiotemporal Impacts of Urban Land Use/Land Cover Changes on Land Surface Temperature: A Comparative Study of Damascus and Aleppo (Syria). *Atmosphere* **2021**, *12*, 1037. [CrossRef]
32. Kamali Maskooni, E.; Hashemi, H.; Berndtsson, R.; Daneshkar Arasteh, P.; Kazemi, M. Impact of spatiotemporal land- use and landcover changes on surface urban heat islands in a semiarid region using Landsat data. *Int. J. Digit. Earth* **2021**, *14*, 250–270. [CrossRef]
33. Rousta, I.; Sarif, M.O.; Gupta, R.D.; Olafsson, H.; Ranagalage, M.; Murayama, Y.; Zhang, H.; Mushore, T.D. Spatiotemporal Analysis of Land Use/Land Cover and Its Effects on Surface Urban Heat Island Using Landsat Data: A Case Study of Metropolitan City Tehran (1988–2018). *Sustainability* **2018**, *10*, 4433. [CrossRef]
34. Ghosh, S.; Kumar, D.; Kumari, R. Assessing spatiotemporal dynamics of land surface temperature and satellite-derived indices for new town development and suburbanization planning. *Urban Gov.* **2022**, *2*, 144–156. [CrossRef]
35. Vision 2030 Website. Available online: https://www.vision2030.gov.sa (accessed on 10 September 2023).
36. Jeddah Municipality Website. Available online: https://www.jeddah.gov.sa (accessed on 10 September 2023).
37. Saudi Arabia Population Statistics 2023. Available online: https://www.globalmediainsight.com/blog/saudi-arabia-population-statistics/ (accessed on 10 April 2023).
38. Elfadaly, A.; Shams Eldein, A.; Lasaponara, R. Cultural Heritage Management Using Remote Sensing Data and GIS Techniques around the Archaeological Area of Ancient Jeddah in Jeddah City, Saudi Arabia. *Sustainability* **2020**, *12*, 240. [CrossRef]
39. Healey, P. Relational complexity and the imaginative power of strategic spatial planning. *Eur. Plan. Stud.* **2006**, *14*, 525–546. [CrossRef]
40. Arif, M.; Gupta, K. Spatial development planning in peri-urban space of Burdwan City, West Bengal, India: Statutory infrastructure as mediating factors. *SN Appl. Sci.* **2020**, *2*, 1–19. [CrossRef]
41. Arif, M.; Aldosary, A.S. Urban Spatial Strategies of the Gulf Cooperation Council: A Comparative Analysis and Lessons Learned. *Sustainability* **2023**, *15*, 13344. [CrossRef]

42. Saudi Arabia Ministry of Economy and Planning (MEP). *Tenth Development Plan, 1437-1440 H (2015–2019) Ninth Development Plan, 1431-1435 H (2010–2014) Eighth Development Plan, 1425–1430 H (2005–2009) Achievements of the Development Plans: Facts and Figures, 1390–1434 H (1970–2013) The Saudi Development March*; MEP: Riyadh, Saudi Arabia, 2009.
43. United States Geological Survey (USGS). Landsat 8 (L8) Data Users Handbook. Available online: https://www.usgs.gov/coresciencesystems/nli/landsat/landsat-8-data-users-handbook (accessed on 10 April 2023).
44. King Abdulaziz Airport Weather Station Information. Available online: https://www.timeanddate.com/weather/saudi-arabia/jeddah/historic (accessed on 10 April 2023).
45. Tamiminia, H.; Salehi, B.; Mahdianpari, M.; Quackenbush, L.; Adeli, S.; Brisco, B. Google Earth Engine for geo-big data applications: A meta-analysis and systematic review. *ISPRS J. Photogramm. Remote Sens.* **2020**, *164*, 152–170. [CrossRef]
46. Gorelick, N.; Hancher, M.; Dixon, M.; Ilyushchenko, S.; Thau, D.; Moore, R. Google earth engine: Planetary-scale geospatial analysis for everyone. *Remote Sens. Environ.* **2017**, *202*, 18–27. [CrossRef]
47. Mutanga, O.; Kumar, L. Google earth engine applications. *Remote Sens.* **2019**, *11*, 591. [CrossRef]
48. Google Earth Engine Platform. Available online: https://code.earthengine.google.com/ (accessed on 1 March 2023).
49. Foody, G.M. Explaining the unsuitability of the kappa coefficient in the assessment and comparison of the accuracy of thematic maps obtained by image classification. *Remote Sens. Environ.* **2020**, *239*, 111630. [CrossRef]
50. El-Hattab, M.; Amany, S.M.; Lamia, G.E. Monitoring and Assessment of Urban Heat Islands Over the Southern Region of Cairo Governorate, Egypt. *Egypt. J. Remote Sens. Space Sci.* **2018**, *21*, 311–323. [CrossRef]
51. Shirani-Bidabadi, N.; Nasrabadi, T.; Faryadi, S.; Larijani, A.; Roodposhti, M.S. Evaluating the Spatial Distribution and the Intensity of Urban Heat Island Using Remote Sensing, Case Study of Isfahan City in Iran. *Sustain. Cities Soc.* **2019**, *45*, 686–692. [CrossRef]
52. Simwanda, M.; Ranagalage, M.; Estoque, R.C.; Murayama, Y. Spatial Analysis of Surface Urban Heat Islands in Four Rapidly Growing African Cities. *Remote Sens.* **2019**, *11*, 1645. [CrossRef]
53. Ranagalage, M.; Estoque, R.; Handayani, H.; Zhang, X.; Morimoto, T.; Tadono, T.; Murayama, Y. Relation between Urban Volume and Land Surface Temperature: A Comparative Study of Planned and Traditional Cities in Japan. *Sustainability* **2018**, *10*, 2366. [CrossRef]
54. Avdan, U.; Jovanovska, G. Algorithm for automated mapping of land surface temperature using Landsat 8 tatellite data. *J. Sens.* **2016**, *2016*, 1–8. [CrossRef]
55. Howard, L. *The Climate of London Deduced from Meteorological Observations*; Cambridge University Press: Cambridge, UK, 2012.
56. Derdouri, A.; Wang, R.; Murayama, Y.; Osaragi, T. Understanding the Links between LULC Changes and SUHI in Cities: Insights from Two-Decadal Studies (2001–2020). *Remote Sens.* **2021**, *13*, 3654. [CrossRef]
57. Qiao, Z.; Wu, C.; Zhao, D.; Xu, X.; Yang, J.; Feng, L.; Sun, Z.; Liu, L. Determining the Boundary and Probability of Surface Urban Heat Island Footprint Based on a Logistic Model. *Remote Sens.* **2019**, *11*, 1368. [CrossRef]
58. Ogashawara, I.; Bastos, V.D.S.B. A Quantitative Approach for Analyzing the Relationship between Urban Heat Islands and Land Cover. *Remote Sens.* **2012**, *4*, 3596–3618. [CrossRef]
59. Kaplan, G.; Avdan, U.; Avdan, Z.Y. Urban Heat Island Analysis Using the Landsat 8 Satellite Data: A Case Study in Skopje, Macedonia. *Proceedings* **2018**, *2*, 358.
60. Wang, R.; Derdouri, A.; Murayama, Y. Spatiotemporal Simulation of Future Land Use/Cover Change Scenarios in the Tokyo Metropolitan Area. *Sustainability* **2018**, *10*, 2056. [CrossRef]

Disclaimer/Publisher's Note: The statements, opinions and data contained in all publications are solely those of the individual author(s) and contributor(s) and not of MDPI and/or the editor(s). MDPI and/or the editor(s) disclaim responsibility for any injury to people or property resulting from any ideas, methods, instructions or products referred to in the content.